HHS Public Access

Author manuscript

Nat Biomed Eng. Author manuscript; available in PMC 2022 November 22.

Published in final edited form as:

Nat Biomed Eng. 2022 February ; 6(2): 129–143. doi:10.1038/s41551-021-00831-9.

Intratumourally injected alum-tethered cytokines elicit potent and safer local and systemic anticancer immunity

Yash Agarwal[1,3], **Lauren E. Milling**[1,3], **Jason Y.H. Chang**[3,4], **Luciano Santollani**[2,3], **Allison Sheen**[1,3], **Emi A. Lutz**[1,3], **Anthony Tabet**[2,3], **Jordan Stinson**[1,3], **Kaiyuan Ni**[3], **Kristen A. Rodrigues**[3,4,7,8], **Tyson J. Moyer**[3,4], **Mariane B. Melo**[3,4], **Darrell J. Irvine**[1,3,4,5,6,8,*], **K. Dane Wittrup**[1,2,3,*]

[1]Department of Biological Engineering, Massachusetts Institute of Technology, Cambridge, Massachusetts, USA 02139

[2]Department of Chemical Engineering, Massachusetts Institute of Technology, Cambridge, Massachusetts, USA 02139

[3]Koch Institute for Integrative Cancer Research, Massachusetts Institute of Technology, Cambridge, Massachusetts, USA 02139

[4]Ragon Institute of Massachusetts General Hospital, Massachusetts Institute of Technology and Harvard University, USA 02139

[5]Department of Materials Science and Engineering, Massachusetts Institute of Technology, Cambridge, Massachusetts, USA 02139

[6]Howard Hughes Medical Institute, Chevy Chase, Maryland, USA 20815

[7]Harvard-MIT Health Sciences and Technology Program, Institute of Medical Engineering and Science, Massachusetts Institute of Technology, Cambridge, Massachusetts, USA 02139

[8]Consortium for HIV/AIDS Vaccine Development, The Scripps Research Institute, La Jolla, California, USA 92037

Abstract

[*]**Correspondence and requests for materials** should be addressed to K.D.W. or D.J.I. wittrup@mit.edu; djirvine@mit.edu.

Author contributions

Y.A., K.D.W. and D.J.I conceived of the study and wrote the manuscript. Y.A. designed the experiments and analyzed data. Y.A., L.E.M., J.Y.H.C., L.S., A.S., E.A.L., A.T., J.S. performed the experiments and data analysis. K.A.R. assisted with the Horiba experiment and K.N. performed the TEM imaging. K.A.R. and T.J.M. provided the AF488-pSer4 peptide and M.D.M provided the plasmid for murine IL15sa.

Reporting Summary. Further information on research design is available in the Nature Research Reporting Summary linked to this article.

Competing interests

Y.A., D.J.I, K.D.W and T.J.M. are named as inventors in patent applications filed by MIT related to the data presented in this work (US20200405950A1). K.D.W. and D.J.I. are cofounders of Ankyra Therapeutics, which has licensed rights to the MIT intellectual property mentioned above.

Supplementary information The online version contains supplementary material available at https://doi.org/10.1038/s41551-01X-XXXX-X.

Antitumour inflammatory cytokines are highly toxic when systemically administered. Here, in multiple syngeneic mouse models, we show that the intratumoural injection of recombinantly expressed cytokines bound tightly to the common vaccine adjuvant aluminium hydroxide (alum) (via ligand exchange between hydroxyls on the surface of alum and phosphoserine residues tagged to the cytokine by an alum-binding peptide) leads to weeks-long retention of the cytokines in the tumours, with minimal side effects. Specifically, a single dose of alum-tethered interleukin-12 induced significant interferon-γ-mediated T-cell and natural-killer-cell activities in murine melanoma tumours, increased tumour-antigen accumulation in draining lymph nodes, and elicited robust tumour-specific T-cell priming. Moreover, intratumoural injection of alum-anchored cytokines enhanced responses to checkpoint blockade, promoting cures in distinct poorly immunogenic syngeneic tumour models and eliciting control over metastases and distant untreated lesions. Intratumoural treatment with alum-anchored cytokines represents a safer and tumour-agnostic strategy to improving local and systemic anticancer immunity.

Immune checkpoint blockade (ICB) therapy has improved progression-free survival in patients suffering from cancer over previous treatment modalities[1–4]. However, ICB typically elicits durable responses in a minority of patients, in part because of the highly immunosuppressive tumour microenvironment (TME)[5,6]. Although rational combinations with inflammatory cytokines or immune agonists can relieve some immunosuppression[7,8], systemic dosing of these proteins is impeded by severe immune-related adverse events (irAE). Early phase 1 clinical trials involving promising cytokines like Interleukin-2 (IL-2) and Interleukin-12 (IL-12) resulted in sub-optimal anti-tumour efficacy with high treatment-related morbidity and even mortality, partially due to limited drug exposure within the tumour and over-stimulation of lymphocytes in healthy tissue[9–14]. Thus, there is great promise for strategies that could localize cytokine effects to the tumour microenvironment.

One approach to focus the activity of immunostimulatory agents in tumours while lowering systemic toxicity is to administer these drugs intratumourally. With advances in interventional radiology, endoscopy and laproscopic surgery procedures, most lesions in the human body are now accessible for intratumoural dosing[15]. Moreover, a locally stimulated immune response in one lesion can elicit systemic anti-tumour immunity to promote control over untreated lesions in patients, especially in combination with systemic checkpoint blockade therapy[16–19]. However, intratumoural injection of therapeutics does not ensure persistence in the TME, since free drugs are quickly cleared via lymphatics and/or the tumour vasculature, rapidly leading to toxic accumulation in the circulation[20,21]. For instance, while there is extensive interest in the local delivery of IL-12[22–24], these approaches are typically accompanied by rapid leakage of IL-12 into the circulation, which in turn triggers systemic interferon-γ (IFN-γ) production (a biomarker for IL-12-related irAEs[25])[26,27]. We have previously reported a strategy of fusing cytokines to collagen-binding proteins to enhance TME retention following intratumoural administration, which reduced toxicities of these potent agents while enhancing therapeutic efficacy[28]. This strategy extends drug persistence over a period of a few days, but is dose-limited by the quantity of collagen available in the TME, which varies from patient to patient and tumour to tumour. Further, drug is spatiotemporally governed by the distribution and turnover of collagen in the tumour.

Here, we demonstrate an approach for the intratumoural delivery of engineered cytokines using the US Food and Drug Administration-approved vaccine adjuvant aluminum hydroxide (alum). Alum has nearly one hundred years of history of safe use in humans and is administered annually to millions of people in over 20 vaccine formulations. Aluminum hydroxide adjuvants are composed of micron-scale aggregates of nanometer-scale rod-shaped nanocrystals; these alum aggregates form a physical depot at injection sites in tissue that is persistent over a period of weeks[29]. Phosphorylated proteins bind tightly to alum through a ligand exchange reaction with surface hydroxyls, enabling retention of bound molecules in the presence of interstitial fluid *in vivo*[30–32]. To exploit this chemistry, we developed an approach for in-cell site-specific protein phosphorylation to synthesize bioactive proteins fused with a phosphorylated alum-binding peptide (ABP) tag. We used this approach to produce a series of ABP-labeled cytokines, which rapidly adsorbed to alum after simple mixing, and upon intratumoural injection were retained in tumours for more than a week. Applied to the cytokine IL-12, this approach dramatically increased intratumoural retention of the cytokine and eliminated systemic toxicities seen upon intratumoural injection of the free drug, while also increasing anti-tumour efficacy. Moreover, a single intratumoural dose of alum-anchored IL-12 elicited strong IFN-γ-dependent collaboration between innate and adaptive immune cells, producing robust systemic anti-tumour responses in multiple poorly immunogenic preclinical models when combined with systemic checkpoint blockade therapy.

Results

Targeted phosphorylation via an in-cell approach is robust

A single kinase, Fam20C, is responsible for phosphorylation of the majority of the mammalian secreted phosphoproteome[33]. We hypothesized that co-expression of Fam20C together with therapeutic proteins fused to a short peptide containing consensus motifs for the kinase (alum binding peptide or ABP hereafter), would lead to the specific phosphorylation of the ABP (Fig. 1a). Fam20C recognizes and phosphorylates serines contained within a well-defined consensus motif (S-x-E) in mammalian cells[33,34], and can be engineered for retention in the endoplasmic reticulum using a KDEL C-terminal tag while still maintaining activity[33]. Thus, we designed an initial set of ABP peptides bearing SXE motifs based on naturally phosphorylated sequences[33] and co-expressed a single-chain form of mouse IL-12 fused to these ABPs together with Fam20C-KDEL in HEK293-F cells (Fig. 1a). The resulting IL-12-ABP proteins were purified by sequential immobilized metal affinity chromatography and anion exchange chromatography (AEC, Supplementary Fig. 1a–h). AEC revealed a major product peak (P3, Supplementary Fig. 1f–h) that was the monomeric, fully-phosphorylated IL-12-ABP. IL-12-ABP was phosphorylated when co-expressed with the kinase (IL-12-ABP-p) but not when expressed without kinase (IL-12-ABP-np), and IL-12 lacking the ABP was not phosphorylated regardless of the presence of the kinase (Fig. 1b–c). Phosphorylation was dependent on the presence of the target serines in the S-x-E motifs and was sensitive to the spacing between these motifs as well as the sequence of flanking residues (Supplementary Fig. 1i–l). When fused to other therapeutic cytokines (IL-2 fused to mouse serum albumin (MSA, to enhance expression) or a superagonist complex of Interleukin-15 (IL-15) with the IL-15α chain (IL-15sa)),

we observed consistent phosphorylation of the ABP (Fig. 1d), indicating that this in-cell Fam20C-dependent phosphorylation approach is robust and modular.

Initial adsorption of IL-12 to alum in buffer was similar irrespective of the presence of the ABP tag (Supplementary Fig. 2a). However, the majority of IL-12 with a phosphorylated ABP remained bound following incubation of the cytokine-loaded alum with mouse serum, while unphosphorylated IL-12 rapidly desorbed (Fig. 1e). Tracked over time, phosphorylated IL-12 was slowly released from alum over ~2 weeks (Supplementary Fig. 2b). IL-12 anchoring on alum increased the size of alum crystal microaggregates in saline (Supplementary Fig. 2c) but the nanoscale morphology of alum nanorods appeared unchanged (Supplementary Fig. 2d–e). Further, the bioactivity of IL-12-ABP-p was similar to native single-chain IL-12 as measured by splenocyte activation (Fig. 1f) and HEK-Blue IL-12 reporter cell activation (Supplementary Fig. 2f–g). Interestingly, IL-12-ABP-p remained functional while adsorbed to alum particles, although with a several-fold reduction in EC50 (Fig. 1f, Supplementary Fig. 2h). The bioactivity of alum-bound IL-12-ABP-p was essentially constant even following multiple days of incubation in serum at 37°C, indicating high *in vitro* stability for alum-cytokine complexes (Supplementary Fig. 2i). We also analyzed *in vitro* alum binding and bioactivity of IL-2-ABP and IL-15sa-ABP fusion proteins. Similar to IL-12, when tagged with the phosphorylated ABP, these cytokines also showed enhanced retention on alum following serum exposure (Supplementary Fig. 2j–k). IL-2-ABP-p exhibited a 4-fold loss in activity when bound to alum similar to IL-12-ABP-p, while IL-15sa-ABP-p showed no change in bioactivity when bound to alum (Supplementary Fig. 2l–m). Thus, ABP-fusion cytokines produced by in-cell phosphorylation exhibit stable alum binding and remain functional while immobilized on alum *in vitro*.

Alum-bound IL-12 safely persists *in vivo* after treatment

We next assessed the biodistribution and pharmacokinetics (PK) of alum-bound IL-12-ABP-p *in vivo*. We previously reported a strategy to stably label alum particles using an AlexaFluor 488 dye conjugated to a solid phase-synthesized poly-phosphoserine ($pSer_4$) peptide[31]. Alum was labeled using this approach and combined with IL-12-ABP-p labeled with AlexaFluor 568 dye. Immediately following intratumoural (i.t.) injection in subcutaneously-implanted B16F10 melanoma tumours, we observed that alum and phosphorylated protein were colocalized and distributed throughout the tumour bed (Fig. 2a). Measurement of IL-12 remaining in tumours 24, 72 or even 144 hours later revealed a >400-fold greater retention of alum-tethered IL-12-ABP-p vs. free IL-12-ABP-p (Fig. 2b). IVIS whole-animal fluorescence imaging of labeled alum-bound IL-12-ABP-p showed persistence of the cytokine at high levels in injected tumours for weeks after a single dosing, while signal from IL-12-ABP-p injected without alum was rapidly cleared (Fig. 2c–d, Supplementary Fig. 3a). Note that the high density of dye-labelled protein bound to alum leads to some fluorescence quenching at time zero[31], which is alleviated over the first few days as some cytokine is released, lowering the dye density and causing an artificial increase in signal over the first few days post injection. I.t. injection of free IL-12-ABP-p or alum mixed with non-phosphorylated IL-12 led to high levels of the cytokine in serum a few hours after treatment, while alum/IL-12-ABP-p injection led to IL-12 levels that were not statistically different than the baseline of untreated mice (Fig. 2e, Supplementary Fig. 3b).

IL-12 induces Interferon-gamma (IFN-γ) secretion by lymphocytes, which has been associated with toxicity in IL-12 clinical trials[35]. To assess the impact of altered IL-12 PK on safety, we established Ag104A fibrosarcoma flank tumours in C3H-Hej mice, which are known to better model human sensitivity to IL-12 than C57Bl/6 mice[35]. Unanchored IL-12 rapidly dispersed in the blood as observed in C57Bl/6 mice (Supplementary Fig. 3c). I.t. injection of free IL-12 or alum mixed with non-phosphorylated IL-12 led to animal weight loss, significant elevations in serum IFN-γ and alanine transaminase (ALT, indicating liver toxicity), and reduced albumin and total protein levels in blood after a single dose (Fig. 2f–h, Supplementary Fig. 3d–f). By contrast, intratumoural injection of alum-anchored IL-12-ABP-p elicited significantly lower serum IFN-γ levels, prevented ALT levels from exceeding the normal clinical range, and left blood chemistry unaffected, correlating to no weight loss in treated animals (Fig. 2f–h, Supplementary Fig. 3d–f). Histopathological analysis of lungs from treated mice, however, didn't reveal further toxicity (Supplementary Fig. 3g). Overall, anchoring of IL-12 to alum through the phosphorylated ABP led to efficient intratumoural retention, substantially improving the systemic tolerability of this potent cytokine.

Anti-tumour efficacy is stronger with i.t. IL-12 retention

Intratumoural dosing of alum-bound IL12 was not only safer but also much more effective. A single i.t. dose of IL12-ABP-p + alum into large subcutaneous Ag104A tumours led to complete responses (CRs) in 11 of 13 animals, while unanchored IL12-ABP-p was only moderately effective and led to treatment-related mortality in 1 of 13 animals (Fig. 3a, Supplementary Fig. 4a).

While many cytokines have unacceptable toxicity when administered systemically, checkpoint blockade antibodies and antibodies against tumour cell surface antigens are better tolerated and are approved as systemic treatments. Thus, we also investigated the anti-tumour efficacy of combining a single intratumoural alum/ABP-cytokine dose with systemic administration of antibodies modeling clinically-relevant treatment combinations. We first treated mice bearing established B16F10 melanoma tumours intratumourally with a single dose of MSA-IL-2 accompanied by systemic administration of an antibody against tyrosinase-related protein 1 (anti-TYRP-1 or TA99). We previously reported that TA99 combined with MSA-IL-2 fused to the collagen-binding protein lumican leads to some curative responses in this model following multiple doses[28]. Alum-bound phosphorylated MSA-IL-2-ABP-p combined with TA99 regressed tumours and elicited complete responses in the majority of treated animals following a single dose (Fig. 3b, Supplementary Fig. 4b–e). By contrast, injection of MSA-IL-2-ABP-p in the absence of alum or administration of alum mixed with unphosphorylated MSA-IL-2 elicited little survival benefit over treatment with the TA99 alone, with no long-term survivors (Fig. 3b, Supplementary Fig. 4b–e). Moreover, a single injection of lumican-MSA-IL-2 in combination with TA99 was significantly less effective than alum-bound IL-2 (Fig. 3b, Supplementary Fig. 4d). The majority of mice that rejected their primary tumours also rejected cancer cells on rechallenge for the IL-2/alum/TA99 combination (Supplementary Fig. 4f).

We next tested intratumoural IL-12 treatment in the same tumour model in combination with anti-PD1 therapy. I.t. alum/IL-12-ABP-p combined with systemic anti-PD1 elicited complete responses in 12 of 23 mice, while unanchored IL-12-ABP-p provided only a modest tumour growth delay and no long-term survival (Fig. 3c, Supplementary Fig. 4g). Notably, anti-PD1 played an important role in the high efficacy of the alum-anchored IL-12/checkpoint blockade combination (Supplementary Fig. 4h). In this study, we also assessed the immunogenicity of IL-12-ABP-p constructs: Compared to the positive control of mice immunized with ovalbumin mixed with alum, no detectable anti-drug antibody responses were detected by ELISA (Supplementary Fig. 4i). In another syngeneic tumour model, the MC38 colon carcinoma, single shot alum/IL-12-ABP-p therapy elicited even stronger responses (9/10 CRs) in combination with systemic anti-PD1, while IL-12-ABP-p in the absence of alum was significantly less potent (Fig. 3d, Supplementary Fig. 4j).

The ability of alum anchoring to block cytokine dissemination into the blood prompted us to next test combinations of alum-bound cytokines. Treatment of B16F10 tumours with a single i.t. dose of alum-tethered MSA-IL-2-ABP-p and IL-12-ABP-p accompanied by systemic anti-PD1 led to tumour eradication in 9 of 10 mice with no weight loss (Fig. 3e–f). By contrast, i.t. administration of this cytokine combination in the absence of alum led to pronounced weight loss and much poorer efficacy (Fig. 3e–f). In summary, by anchoring cytokines to alum via phosphorylation, both the safety and anti-tumour efficacy are enhanced in diverse tumour models, and clinically-relevant combination treatments achieve high levels of therapeutic efficacy following a single i.t. injection.

Alum-cytokine treatment promotes control over distal lesions

The success of any intratumoural therapy in the clinic will depend on its ability to promote systemic anti-tumour responses to control distal, untreated lesions and micro-metastases[16,36]. Therefore, we tested the ability of single-shot alum-IL-12 therapy to promote abscopal responses using two distinct models. First, we established Ag104A tumours on opposite flanks of mice and treated only one of the tumours with a single dose of alum with anchored IL-12-ABP-p (Fig. 4a). Even though IL-12 leakage into the blood was eliminated by alum binding, single dose IL-12-ABP-p/alum exhibited greater efficacy than IL-12 alone, and elicited a systemic response that eliminated established distal untreated tumours in the absence of systemic checkpoint blockade therapy (Fig. 4b–f). Alum-anchored IL-12-ABP-p also significantly outperformed free IL-12-ABP-p in mice with bilateral B16F10 tumours in combination with systemic anti-PD-1(Supplementary Fig. 4k–l).

A second important clinical treatment scenario is neoadjuvant therapy. To assess the potential of alum-bound cytokines to be effective in this setting, we orthotopically implanted spontaneously metastatic 4T1 breast cancer cells in the mammary fat pad of BALB/c mice, and treated established tumours with a single dose of alum, IL-12-ABP-p or IL-12-ABP-p + alum, in combination with systemic anti-PD1. Nine days after treatment, we surgically resected the primary tumours and monitored the mice for survival (Fig. 5a). Alum-bound IL-12-ABP-p significantly slowed primary tumour progression relative to treatment with alum alone or free IL-12-ABP-p (Fig. 5b). In this model, animals are susceptible to relapse

due to micrometastases in the lungs. The combination of alum-bound IL-12-ABP-p and anti-PD1 led to long-term survival of ~75% of animals, in contrast to minimal benefit achieved by alum/anti-PD1 or IL-12/anti-PD1 (Fig. 5c). To evaluate whether this Supplementary survival was due to improved tumour-specific T cell responses, we analyzed the peripheral blood of all survivor mice for the frequency of $CD8^+$ T cells specific to gp70, an endogenous retroviral antigen expressed by 4T1 cells[37]. Impressively, a single dose of alum-anchored IL-12 promoted high gp70 tetramer$^+$ T cell responses over both age-matched untreated mice bearing orthotopic 4T1 tumours and the few long-term survivors treated with free IL-12-ABP-p (Fig. 5d–e). Thus, a single dose of alum-anchored IL-12 elicits systemic immunity enabling control over non-injected distal tumours in multiple tumour models.

Alum/IL-12-induced IFN-γ drives early tumour regression

IL-12 can activate cells from both the innate and adaptive immune compartments either directly or indirectly via IFN-γ[10,22,38–40]. To determine the cellular and molecular effectors implicated in the context of persistent intratumoural IL-12, we first carried out quantification of cytokines and chemokines generated in the TME of B16F10 tumours. Three days post treatment, alum/IL-12-ABP-p upregulated a battery of inflammatory effector proteins including IL-6, TNF-α, IL-1β, CXCL9, and CXCL10 (Fig. 6a, Supplementary Fig. 5a–b). By this timepoint, IFN-γ production was increased 5-fold over treatment with alum alone or IL-12-ABP-p alone, and was sustained for at least 6 days (Fig. 6b), indicating that high amounts of intratumourally-retained IL-12 are still active at this time point. Although alum is known to activate the NLRP3 inflammasome[41], cytokine release in tumours and anti-tumour efficacy were unaffected in *Nlrp3*$^{-/-}$ mice (Supplementary Fig. 5c–g).

Successful checkpoint blockade therapy in mice relies on strong collaboration between T cell-produced IFN-γ and dendritic cell (DC)-produced IL-1238. Here, treatment in the presence of an IFN-γ-neutralizing antibody entirely eliminated the efficacy of alum-anchored IL-12 with immediate loss of tumour control (Fig. 6c, Supplementary Fig. 6a). Thus, we asked what key cellular effectors drive IFN-γ expression in response to IL-12 (Supplementary Fig. 7). While IFN-γ production was upregulated in multiple cell types by alum-anchored IL-12, $CD8^+$ T cells and NKT cells made up roughly 88% of the IFN-γ-producing cells in the treated tumour, and alum-bound cytokine substantially increased IFN-γ production by these two populations relative to IL-12 alone (Supplementary Fig. 6b–d). Immunohistochemical analysis of treated B16F10 tumours in IFN-γ reporter mice[38] revealed that alum-IL-12-ABP-p treatment but not free IL-12-ABP-p induced pockets of IFN-γ^+ $CD8^+$ T cells deep in tumour lesions (white arrows, Fig. 6d), and in some regions IFN-γ^+ $CD8^+$ T cells appeared to interact directly with fluorescently labelled IL-12-ABP-p one week after treatment (yellow arrows, Supplementary Fig. 6e). Antibody-mediated depletions revealed that CD8α $^+$ cells are critical to early tumour control and long-term immunity, while NK1.1$^+$ cells did not have a statistically significant impact on therapeutic efficacy (Fig. 7a, Supplementary Fig. 8a, 9).

While we found no significant difference in tumour immune cell infiltration three days after i.t. injection of free vs. alum-anchored IL12 (Fig. 7b, Supplementary Fig. 8b), alum-bound IL12 induced a substantial IFN-γ^+Granzyme B^+ $CD8^+$ T cell population with upregulated

granzyme expression by 3 days after treatment, and similar trends in $CD4^+$ T cells, NK cells and NKT cells (Fig. 7c–e, Supplementary Fig. 8c–e). Over time, alum/IL-12 established a significantly higher CD8/Treg ratio in the tumour over unanchored IL-12 (Fig. 7f) and these infiltrating $CD8^+$ T cells showed higher expression of CD25 and CD107a over treatment with free IL-12-ABP-p in the tumour as long as 9 days after treatment (Fig. 7g–h, Supplementary Fig. 8f). Thus, a single dose of alum-anchored IL-12 induced effector responses from innate (NK, NKT) and adaptive ($CD8^+$, $CD4^+$ T cells) immune cells, but $CD8^+$ T cells and IFN-γ are critical for ultimate tumour control.

Alum/IL-12 boosts antigen uptake in draining lymph node

Alum-bound IL-12 induced rapid upregulation of IFN-γ expression from tumour-infiltrating T cells early after treatment, but the observation of immunological memory (Supplementary Fig. 4f) and sustained tumour antigen-specific T cell responses (Fig. 5d–e) suggested that ultimate disease control may involve priming of *de novo* T cell responses. We treated established B16F10 tumours in *Batf3*$^{-/-}$ animals lacking cross-presenting DCs[42] that are crucial for priming T cells against tumour antigens, and long-term survival after i.t. therapy was significantly reduced in these mice (Fig. 8a). To track tumour antigen uptake by DCs, we treated B16F10 tumours expressing the stable fluorescent protein Zsgreen[43] and analyzed draining lymph nodes (dLN) by flow cytometry (Supplementary Fig. 10). $CD103^+$ cDC1s were previously reported to be critical antigen-carrying cells for T cell priming in the B16F10 tumour model[43,44]. While the infiltration of DC and other myeloid cell populations remained relatively unchanged within treated tumours (Supplementary Fig. 11a–b), activated, antigen-loaded $CD103^+$ DCs steadily increased over time only in the dLNs of alum/IL-12-ABP-p-treated animals (Fig. 8b–c). Further, injection of free IL-12-ABP-p without alum led to only slight transient increases in CD86 and MHC-II expression, but alum-anchored IL-12-ABP-p maintained this upregulation of CD86 and MHC-II in dLN $CD103^+$ DCs even 6 days after treatment, moving a large proportion of these cells into a more persistent $CD86^{hi}MHC\text{-}II^{hi}$ state (Fig. 8d, Supplementary Fig. 11c).

Antibody-mediated depletions show that $CSF1R^+$ macrophages and monocytes also impacted long-term survival, while $Ly6G^+$ neutrophils did not (Fig. 8e). While both anchored and unanchored IL-12-ABP-p upregulated MHC-II and CD86 in tumour-infiltrating monocytes (Supplementary Fig. 11d–e), alum-bound IL-12-ABP-p expanded a greater dLN-infiltrating $MHC\text{-}II^+$ and $CD86^+Zsgreen^+$ monocyte population in draining lymph nodes, which peaked 3 days post treatment (Fig. 8f–g, Supplementary Fig. 11f–g). IL-12-ABP-p + alum also promoted CD11c expression in dLN monocytes, suggesting their differentiation toward monocyte-derived DCs (Fig. 8h). Other DC and macrophage populations in the dLNs, particularly migratory $CD11b^+$ DCs (cDC2s) and medullary chord macrophages (MCM), also had higher levels of CD86 and Zsgreen uptake over time after treatment with alum-bound IL-12-ABP-p (Supplementary Fig. 11h–j). Consistent with these shifts in antigen uptake in APCs, an IFN-γ enzyme-linked immune absorbent spot (ELISPOT), performed on irradiated B16F10 cells cultured with splenocytes harvested 10 days after i.t. treatment of B16F10 tumours revealed significantly higher tumour-specific responses in mice treated with alum/IL-12-ABP-p than those treated with IL-12-ABP-p alone (Fig. 8i). In summary, by tethering IL-12 to alum and improving its intratumoural

persistence following a single dose, several antigen presenting myeloid cell types remain highly activated while presenting antigen in tumour dLNs and enhancing tumour-specific T cell priming.

Discussion

Clinical translation of cytokine-based cancer immunotherapy has been challenging. To date, only IFNα and IL-2 have been approved by the US FDA for use in certain indications and even those have fallen out of favor due to toxicity concerns[45]. IL-12 potently drives anti-tumour immunity in mouse models but has been found to have an unmanageably narrow therapeutic window in humans[22]. Here, we report a modular approach for the local delivery of high dose-cytokine therapy with negligible toxicity. A single i.t. dose of alum-anchored cytokines enabled *in situ* vaccination, promoting durable local and systemic anti-tumour responses in several mouse cancer models.

Although other biomaterials such as injectable hydrogels[46–49], polymeric microspheres[48], Montanide ISA-51[51], mesoporous silica nanoparticles[52], microneedle patches[53,54] and other materials[22,55,56] have been explored for the local and sustained release of cytokines and chemokines in tumours, the FDA approval for use of these approaches in cancer remains a constant hurdle due to regulation, manufacturing and scalability challenges[57]. Further, precise engineering of the release rate of drugs to match their consumption rate in tumours has been extremely difficult, with clear evidence of drug leakage into the systemic circulation for most of these platforms[46,49]. For IL-12 in particular, there is significant interest in the intratumoural delivery of the IL-12 gene either via plasmid electroporation[58] or several viral and non-viral vectors[26,27]. However, this strategy also often results in the swift accumulation of IL-12 and IFN-γ in the blood[22]. By anchoring IL-12 to alum using phosphorylated peptide tags, we are able to dramatically limit such systemic dissemination, while maintaining high efficacy.

The number of clinical trials involving intratumoural immunotherapy has increased swiftly over the last decade, and the oncolytic viral therapy TVEC became the first FDA approved local immunotherapy in 2015. With innovations in interventional radiology and surgical techniques, essentially any lesion has become accessible for intratumoural injections, making human intratumoural immunotherapy a viable route for the administration of cancer drugs[62]. However, for lesions requiring surgery, treatments that can elicit prolonged immunostimulation following infrequent injections will be desirable, in combination with systemic dosing of approved therapies such as checkpoint blockade or tumour-targeting antibodies. In the single i.t. dose context, we show that alum-anchored IL-2 and IL-12 can greatly improve outcomes in both immunologically “hot” (MC38) and “cold” (B16F10) tumours in combination with checkpoint blockade or anti-tumour antibodies. We also see improved survival over collagen-anchored IL-2 in the single dose setting. Strikingly, a single local dose of IL-12 also elicited systemic responses, delaying the growth of established untreated distal tumours in two different solid tumour models and greatly decreased lung metastases after neoadjuvant treatment of orthotopic 4T1 tumours, a model for triple-negative breast cancer.

Whereas enhancing intratumoural residence of IL-12 led to the expected stimulation of T cells and NK cells to produce IFN-γ, we also observed significant activation of APC populations in draining lymph nodes, and increased tumour antigen accumulation in these cells. This effect could result from direct IL-12 signalling[40,59], IFN-γ -mediated reprogramming of DCs and monocytes[60,61] or an indirect outcome of tumour antigen and DAMP release following cancer cell killing triggered by IFN-γ and Granzyme B-producing T and NK cells. MHC-I upregulation by tumour cells after IFN-γ release is expected to promote cytolytic T cell killing. Antibody-mediated neutralization experiments indicated that while early tumour control may be entirely dependent on IFN-γ-driven immune responses, long-term tumour regression required both innate (cDC1, CSF1R+ monocytes and macrophages) and adaptive (CD8+ T cells) immune cells. The observed reprogramming of intratumoural monocytes might also contribute to increased tumour-cell killing. Thus, by tethering IL-12 to alum for i.t. treatment, we not only restrict toxicity but also potentiate IL-12's pleiotropic therapeutic mechanisms of action.

Alum mixed with IL-12 was previously used to promote Th1 responses to sub-unit vaccines[63,64]. We used alum for the multiday persistent delivery of cytokines to tumours. In the vaccine context, alum has been reported to improve humoral immunity by enabling sustained retention of antigen at injection sites, improving uptake by antigen-presenting cells, promoting necrosis and release of DAMPs at the injection site and signal through the NLRP3 inflammasome to elicit type 2 helper T cell (Th2)-based antibody responses[32]. We found, however, that the NLRP3 inflammasome was not necessary for either inflammatory cytokine release or overall therapeutic efficacy for single-dose alum-IL-12 therapy. Some release of IL-6 and TNF-α does occur with i.t. treatments of just alum one day after treatment. This could be attributed to alum promoting necrosis in the tumour. However, this inflammation was only transient since i.t. injections of alum alone never led to substantial tumour control in any of the models we tested. Site-specific anchoring of proteins to solid surfaces can enhance stability and protect from endogenous, extracellular proteases. So, alum may also delay cytokine degradation *in vivo* and enhance the signaling period for cytokines[65].

In this study, we report the retention of alum-bound cytokines at injection sites for weeks after administration. Further, therapeutic efficacy appears to rely on strong activation driven by early IL-12 retention with enhanced IFN-γ secretion in the tumour lasting at least a week after treatment. Although delayed-type hypersensitivity to alum is rare and clinically manageable in humans[66], and we did not observe anti-ABP or anti-cytokines antibodies in treated animals, chronic inflammation due to long-term cytokine release at the sites of cured tumours could promote autoimmune reactions and granulomas[67]. Thus, it will be of interest in future work to define an optimal window for cytokine signaling and evaluate the long-term degradation, accessibility and bioactivity of the alum-cytokine depot. If there is active, accessible IL-12 months after treatment, alterations in the ABP designs such as the addition of a protease cleavage tag or a pH-responsive linker[68] could be made to ensure the removal of the cytokine after primary tumour cure.

The intracellular Fam20c phosphorylation method was developed with manufacturability and generalizability in mind[31]. For biomanufacturing generality and to take advantage of

highly developed GMP cell expression platforms, we developed an in-cell phosphorylation strategy such that proteins are modified during secretion from mammalian cells. Stable cell lines expressing Fam20C could be next used for the transient transfection of any ABP-fusion protein of interest. Further, even proteins with internal S-x-E sites (IL-12p40 has two S-T-E sites) were only phosphorylated with the ABP present, indicating that the clustering of the motifs on one unstructured small peptide dominates phosphorylation. With some optimization in ABP design, linker sequence between ABP and target protein, and position of ABP within the protein, we have been able to apply this approach to antibodies, antibody-cytokine fusion proteins, other cytokines such as interferons and other interleukins.

Finally, effective temporal programming may be critical to harnessing the true power of combination immunotherapy[69]. The customizability of the ABP approach may enable one to precisely control and tune release of proteins from alum *in vivo* and eventually, program timing such that a single shot of alum-anchored proteins would lead to release of distinct therapies at different times after treatment.

Methods

Cell Lines and Animals

Cell lines B16F10 (ATCC), HEK-Blue IL-12 (Invivogen), HEK293-F (Gibco), 4T1 (ATCC) and CTLL-2 (ATCC) cells were cultured following vendor instructions. 4T1-GFP-Luc (4T1-Luc) cells were generated by transfection of the 4T1 cell line with pGreenFire lentiviral vector (System Biosciences) and B16F10-Trp2 KO cells were generated as previously described (Moynihan et al). Ag104A, MC38 and B16F10-Zsgreen cells were a gift from H. Schreiber (University of Chicago), J. Schlom (National Cancer Institute) and R. Hynes (MIT) respectively. 4T1 cells were cultured in Roswell Park Memorial Institute (RPMI) 1640 media (ATCC) supplemented with 10% fetal bovine serum (FBS), 100 units/ml penicillin and 100 ug/ml streptomycin while Ag104A, MC38 and B16F10-Zsgreen were all cultures in complete Dulbecco's Modified Eagle's Medium (DMEM) supplemented with 10% fetal serum (FBS), 100 units/ml penicillin and 100 ug/ml streptomycin. All cells were maintained at 37C and 5% CO_2, and all tested negative for mycoplasma.

Female C57BL/6 (Taconic, C57BL/6NTac), Balb/C (JAX, 000651), *Batf3*$^{-/-}$ (JAX, 013755), *Nlrp3*$^{-/-}$ (JAX, 021302), albino B6 (JAX, 000058), C3H/Hej (JAX, 000659) and IFNγ-reporter GREAT (JAX, 017581) mice at 6–10 weeks age were purchased and maintained in the animal facility at the Massachusetts Institute of Technology. All animal studies and procedures were carried out following federal, state and local guidelines under an institutional animal care and use committee-approved animal protocol by the Committee of Animal Care at MIT.

Cloning, Protein Purification and Phosphorylation Analysis

Genes for single chain IL-12 and MSA-IL-2 proteins were cloned into the gWiz vector (Genlantis) as previously described[28]. Murine version of IL-15sa was designed based on the human clinical candidate ALT-803 by replacing the sushi domain of the human IL-15 receptor alpha and human IL-15 sequences by those from mouse. Chimeric

(sushiIL-15Rα-IL-15) sequences were synthesized as gBlock gene fragments (Integrated DNA technologies) and cloned into the gWiz vector. The sequences for ABP10 was designed based on previously reported successfully phosphorylated peptides[33]. SEE was the most abundant naturally phosphorylated motif and the flanking residues determined were those that were repeated atleast twice in the panel. All alum binding peptides (ABP) were ordered as gBlock gene fragments or single-stranded DNA primers (Integrated DNA technologies) that were then cloned into IL-12, MSA-IL-2 or IL-15sa containing gWiz vectors by In-Fusion (Takara Bio Inc.) such that all ABP-containing proteins would have poly-Histidine (His) tags. Site-directed mutagenesis was done via simple mutations in primers followed by PCR. Human cDNA for Fam20C (Horizon, previously DharmaCon) was also cloned into gWiz with a terminal KDEL tag (without a His tag). All plasmids were transformed into Stellar Competent Cells (Takara Bio Inc.) and purified using the NucleoBond Xtra Maxi EF endotoxin-free maxi-prep kit (Takara Bio Inc.).

For protein production, plasmids were transiently transfected into HEK293-F cells (1 mg total DNA/L cell culture) via polyethylenimine (2 mg/L cell culture) using the Freestyle 293 Expression system (Gibco). For all co-transfections, target protein plasmid:Fam20C plasmid transfection mass ratio was restricted to 9:1. TA99 was purified using rProtein A Sepharose Fast Flow resin (Cytiva Life Sciences, formerly GE Healthcare) as described previously[8]. His-tagged proteins from cell culture supernatants were then purified using HisPur Ni-NTA metal affinity resin (ThermoFisher Scientific). Monomeric phosphorylated proteins were further purified using custom anion exchange chromatography salt gradients (Supplementary Data Fig 1) on HiTrap Q HP columns attached to an AKTA FPLC system (Cytiva Life Sciences, formerly GE Healthcare). Proteins were buffer exchanged into Tris-Buffered Saline (1X, Sigma-Aldrich) using appropriate Amicon spin columns (Sigma-Aldrich). Purified proteins were confirmed to have low endotoxin levels (<0.1EU per dose) by the Endosafe Nexgen-PTS system (Charles River) and validated for size by SDS-PAGE and phosphorylation by a malachite green assay (Pierce Phosphoprotein Phosphate Estimation Assay Kit, ThermoFisher Scientific). Further validation of phosphorylation was done by western blot. Briefly, proteins were run on a NuPAGE gel in MES, transferred onto a nitrocellulose membrane using the iBlot system (Invitrogen). The membrane was blocked by 0.5X Odyssey blocking buffer (LI-COR), and then stained with a rabbit anti-pSer antibody (Abcam, ab9332, 1:125) and anti-rabbit IR800 antibody (LI-COR, 1:10000).

In vitro alum binding and bioactivity assays

All alum used in the study was Alhydrogel purchased from Invivogen. Alum-binding assays were performed as described previously31. Briefly, proteins were conjugated to Alexa Fluor 647 (AF647) via NHS labelling (Invitrogen), mixed with alum with a mass ratio of 10:1 alum:protein unless otherwise noted in TBS and rotated at room temperature (RT) for 20 minutes to enable adsorption. Subsequently, the samples were centrifuged at 10,000xg for 10 minutes to pellet alum and the supernatant was aliquoted and replaced with 10% mouse serum-containing PBS. The tubes were then moved to a rotator at 37°C. At indicated time points, the samples were removed, centrifuged and the supernatant was replaced with free 10% mouse serum-containing PBS. All removed supernatants were analyzed for

fluorescence using a Tecan Infinite M200 Pro absorbance/fluorescence plate reader and the results were normalized to samples that had no alum.

All bioactivity assays were performed in U-bottom plates to maximize alum-protein-cell interactions. For IL-12 bioactivity, two *in vitro* assays were used – HEK-Blue IL-12 reporter assay and *ex vivo* splenocyte stimulation assay. The HEK-Blue assay (Invivogen) was run according to manufacturer's instructions with 5:1 alum:IL-12 mass ratio. For serum stability assay, alum/IL-12 mixtures were incubated in TBS supplemented with 20% FBS for the indicated time before adding to cells. For the splenocyte assay. Spleens were harvested from C57BL/6 mice and processed into single cell suspensions. Red blood cells were lysed with ACK lysing buffer (Gibco) and splenocytes plated in a 96-well plate at 500,000 cells/well. Then, IL-12, IL-12-ABP-p, IL-12-ABP-p + alum or just alum were added at indicated concentrations and incubated with splenocytes for 48 hours at 37°C. Supernatants were diluted 3x and analyzed for IFNγ via ELISA (Mouse IFNγ DuoSet ELISA, R&D Systems). Culture medium was RPMI supplemented with 10% FBS, 1% penicillin-streptomycin, 1X non-essential amino acids (Invitrogen), 1X sodium pyruvate (Invitrogen), 1X 2-mercaptoethanol (Invitrogen) and 10 ng/mL mouse IL-2. For IL-2, IL-15 bioactivity, 10,000 CTLL-2 cells were plated in incomplete media (no T-STIM w/ ConA) with indicated concentrations of recombinant MSA-IL-2 or IL-15 proteins with or without alum and incubated for 48 hours at 37°C. Mass ratio used was 2.5:1 and 5:1 alum:protein for MSA-IL-2 and IL-15 respectively. Cell viability was determined via the ATP-detecting CellTiter-Glo 2.0 assay (Promega) as per manufacturer's instructions. Luminescence was measured using the Tecan plate reader with 0.25s integration time.

Morphology and Size Characterization of alum/cytokine particles

Transmission electron microscopy was used to analyze morphology of particles. 10 uL of premixed alum/IL-12 or alum alone were dropped on 200 mesh copper grids coated with a continuous carbon film and dried at room temperature. Grids were then mounted on a JEOL single tilt holder equipped in the JEOL 2100 FEG microscope. The microscope was operated at 200 kV and with a magnification in the ranges of 10,000~60,000 for assessing particle size and distribution. All images were recorded on a Gatan 2kx2k UltraScan CCD camera.

The size of alum-bound protein particles was assessed using a Horiba Partica LA-950V2 Laser Diffraction Particle Size Distribution Analyzer with the FractionCell Ultra-small Volume Solvent Resistant Cuvette.

Histopathology Analysis

C3H/Hej mice (n=3) were left untreated or treated subcutaneously with 20 ug IL-12-ABP-p alone or mixed with 100 ug alum. 3 days after treatment, lungs and livers of the mice were collected and fixed in 10% formalin. The organs were embedded in paraffin and blocks were cut into 4 um sections followed by haematoxylin and eosin staining. The slides were imaged using the Aperio Digital Slide Scanning System (Leica). The slides were then blindly assessed for tissue damaged by the pathology, Dr. Roderick Bronson.

IVIS

Albino B6 mice were inoculated with one million apigmented B16F10-Trp2 KO cells subcutaneously on the right flank. After the tumours became palpable (day 6), tumours were intratumourally treated with 30 uL of AF647-labelled proteins mixed with alum. For IL-12, 20 ug (~316 pmol) of protein (IL-12, IL-12-ABP, IL-12-ABP-p) was mixed with 100 ug alum in TBS and rotated in the dark at RT for 20 minutes before administration. After treatment, mice were imaged with the IVIS Spectrum imaging system (Perkin Elmer) under 0.5s exposure epi-illumination fluorescence settings. Image analysis was done using Living Image (Caliper Life Sciences) and data was normalized to maximum radiance throughout the experiment per protein.

Tumour inoculation and intratumoural therapy for subcutaneous flank models

For single-tumour efficacy experiments, 10^6 B16F10, Ag104A or MC38 cells in 50 uL sterile PBS were inoculated on the shaved right flank of mice (B6 for B16F10, MC38 and C3H for Ag104A). At day 6 after tumour inoculation for B16F10 or day 7 for MC38/Ag104A, tumours were treated intratumourally with a 30 uL injection. For all IL-12 treatments, 20 ug of IL-12-ABP-p was used (316 pmol) and the alum:protein mass ratio was 5:1 (20 ug IL-12: 100 ug alum). On the other hand, IL-2 treatment was limited to 36 ug of MSA-IL-2-ABP-p (409 pmol, Fig 3A) or 40 ug of MSA-IL-2-ABP-p (454 pmol, Fig 3G) and the alum:protein mass ratio was 2.5:1. For all experiments, cytokines and alum was pre-mixed in TBS and rotated at RT for 20 minutes before administration. TA99 and aPD1 (clone 29F.1A12, BioXCell) were administered at 200 ug per dose in PBS intraperitoneally (i.p.) when indicated. Tumour area was measured by computing the product of the length and width of flank tumours, and mice were euthanized when the tumour area exceeded 100 mm^2 or if weight loss increased beyond 20%. For rechallenge experiments, 10^5 tumour cells were inoculated on the left flank of mice that rejected primary tumours.

For the Ag104A bilateral tumour model, one million Ag104A cells were inoculated on the right flank of C3H mice while 3×10^5 tumour cells were inoculated on the left flank on the same day. For the B16F10 bilateral tumour model, one million B16F10 cells were inoculated on the right flank of B6 mice while 5×10^5 cells were inoculated on the left flank 3 days after. I.t. treatments for both models occurred in the tumour on the right at day 6 for B16F10 and day 7 for Ag104A. Mice were euthanized when either tumour area exceeded 100 mm^2 or if weight loss increased beyond 20%.

IFN-γ ELISPOT

C57BL/6 mice (n = 5 animals per group) bearing 25mm^2 B16F10 tumours (~day 6 after 10^6 cells were inoculated in the flank) were treated with no i.t. treatment, 100 ug alum i.t., 20 ug IL-12-ABP-p i.t. or 20 ug IL-12-ABP-p + 100 ug IL-12-ABP-p along with 200 ug anti-PD1 i.p. on days 6, 9, 12 and 15. On day 16 (10 days after i.t. treatment), spleens were isolated from mice, mechanically digested through 70 um nylon cell strainers to prepare single-cell suspensions in RPMI supplemented with 10% FBS, 1% penicillin-streptomycin, 1X non-essential amino acids (Invitrogen), 1X sodium pyruvate (Invitrogen), 1X 2-mercaptoethanol (Invitrogen). Red blood cells were lysed in ACK Lysis Buffer (Gibco). On the same day, B16F10 cells (treated with 500 U/mL IFN-γ overnight) were subjected to 120Gy radiation

and then, trypsinized into a single cell suspension in the same supplemented RPMI. 25,000 irradiated B16F10 cells were mixed with 2.5×10^5 splenocytes per sample and seeded in a 96-well ELISPOT plate (BD Biosciences) that was pre-coated with IFN-γ capture antibody (BD Biosciences). Plates were wrapped in foil and cultured for 24 hrs in a 37C incubator, then developed according to the manufacturer's protocol. Plates were scanned using a CTL-ImmunoSpot Plate Reader and data were analyzed using CTL ImmunoSpot Software.

Depletion studies

Depletions of immune cells were done using antibodies against CD8α (clone 2.43, BioXCell 400 ug i.p. twice weekly), NK1.1 (clone PK136, BioXCell, 400 ug i.p. twice weekly), Ly6g (clone 1A8, BioXCell, 400 ug i.p. twice weekly) or CSF1R (clone AFS98, BioXCell, 300 ug i.p. every other day) as previously described[26]. Cytokine neutralization was done using i.p. treatments with 200 ug of antibodies against IFN-γ (clone XMG1.2, BioXCell), IL1β (clone B122, BioXCell) and IL18 (clone YIGIF74-1G7, BioXCell) every other day. All depletion antibodies dosing was initiated one day before i.t. treatment and continued till atleast 1 month after treatment.

Tumour inoculation, treatment and surgery for 4T1 orthotopic model

5×10^5 4T1-Luc tumour cells were inoculated into the fourth mammary fat pad of BALB/c mice and palpable tumours 5 days after inoculation were treated i.t. with 20 ug IL-12-ABP-p, 100 ug alum or a mixture of the two. Mice were also treated with 200 ug aPD1 i.p. on days 5, 8 and 11. Nine days after i.t. treatment (day 14), mice were anaesthetized with isoflurane and provided pre-operative subcutaneous sustained-release buprenorphine (1 mg/kg, ZooPharm) and meloxicam (5 mg/kg). The shaved surgical area was cleaned with alternating swabbing of betadine scrub and ethanol wipes. The primary tumour and draining inguinal lymph node were surgically removed using autoclaved surgical instruments (Braintree Scientific) and the wound was closed with surgical clips. Inguinal lymph nodes were removed due to primary tumours frequently growing around the node; therefore, the inguinal lymph node was removed in all mice. Meloxicam (5 mg/kg) was dosed every 24 hours for 3 days post-op. Mice were then monitored every other day and euthanized if signs of distress, >20% body weight loss, or poor body condition were observed.

ELISA, Luminex and blood chemistry analysis

To analyze anti-drug antibodies after treatment in mice, blood was collected by submandibular bleeding from mice with long-term tumour rejection after treatment with IL-12-ABP-p + alum into Z-gel clotting tubes (Sarstedt). The tubes were centrifuged at 10,000x g for 5 mins and separated serum was stored at −80°C. Serum for control B6 mice was collected 3 weeks after subcutaneous treatment with 20 ug Ovalbumin (OVA, Sigma-Aldrich) adsorbed to 100 ug alum. MaxiSorp Immuno plates (Thermo Fisher) were coated with 2 ug/mL of OVA or IL-12-ABP-p in PBS at 4°C for two days. This was followed by 2 hr RT blocking with PBSA (PBS + 1% Bovine Serum Albumin). Subsequently, serial dilutions of collected serum in PBSA was performed and samples were transferred to the coated plates for another 2 hr RT incubation. Plates were washed with PBS-Tween between every incubation step. Then, anti-mouse IgG-HRP antibody (Biolegend, 5000x) was added

to the wells for a 1 hr RT incubation. Finally, the plates were developed for 20 minutes with TMB (ThermoFisher Scientific) followed by the addition of concentrated sulfuric acid to stop the reaction. Absorbance was measured at A450 (background subtracted by A540) by the Tecan plate reader.

For cytokine/chemokine analysis of serum and tumour lysate, blood was collected at indicated times as described earlier while tumours were collected and ground in tissue protein extraction reagent (T-PER, ThermoFisher Scientific, 78510) with 1% Halt protease and phosphatase inhibitors (ThermoFisher Scientific, 78442). The lysates were incubated with tissue at 4°C for 30 minutes with rotation and then, centrifuged to remove debris. Supernatant was subsequently filtered using Corning Costar SpinX columns before flash-freezing in liquid nitrogen. Amounts of IL-12 and IFNγ in the samples were estimated by ELISA kits from ThermoFisher Scientific(IL-12, 88-7121-22) and R&D Systems(IFNγ, DY485-05) as per manufacturer instructions. Lysates were also sent to Eve technologies (for a 31-plex Luminex analysis) or analyzed in-house using the 13-plex Mouse Macrophage/Microglia Legendplex Panel (Biolegend). Protein amounts (normalized by mass of tumour analyzed) were clustered by Cluster 3.0 developed by M. Eisen at Stanford University and the heatmap was generated by TreeView 3.0. Serum samples were sent to IDEXX Reference Laboratories for analysis of ALT, BUN, Albumin and Total Protein.

Immunohistochemistry of alum-treated tumours

To stain for alum particles independently from ABP-fusion proteins, we relied on fluorophore-conjugated pSer peptides synthesized as described previously[31]. For Fig 2A, B16F10 tumours were treated i.t. with premixed 20 ug AF568-IL-12-ABP-p, 0.4 nmol AF488-pSer4 and 100 ug alum, and treated tumours were removed 30 min after treatment. For Fig 5d and Supplementary Data Fig 6e, B16F10 tumours established in IFNγ-YFP GREAT mice were treated i.t. with premixed 20 ug AF405-IL-12-ABP-p, 0.4 nmol Cy3-pSer4 and 100 ug alum, and tumours were removed 7 days after treatment. For both instances, tumours were fixed with 4% paraformaldehyde overnight, washed and embedded in a 3 wt% low melting point agarose at 37°C, which was then cooled and allowed to solidify on ice for 15 min. 100 um sections were prepared using a Vibratome (Leica VT1000S) and suspended in ice-cold PBS before transferring into a blocking solution containing 10% goat serum, 0.2% Triton-X100 and 0.05% sodium azide overnight at 37°C before staining. For Fig 2A, sections were stained with AF647 TA99 while for sections from GREAT mice, staining was done with APC anti-mouse CD8α Ly 2 (clone CT-CD8a, Cedarlane). Antibodies were diluted 1:100 in blocking buffer overnight at 37°C, followed by washes with 0.05% Tween-20 in PBS and mounted on a glass slide with ProLong Diamond antifade mounting medium (ThermoFisher Scientific). Images were acquired using a Leica SP8 laser scanning confocal microscope with a 25X water objective or 63X oil objective. Images were processed with the Fiji software.

Antibodies, staining and FACS analysis

Antibodies to CD8α (53–6.7), CD103 (2E7), Ly6C (HK1.4), F4/80 (BM8), CD11b (M1/70), CD86 (GL1), MHC2 or I-A/I-E (M5/114.15.2), CD24 (30-F1), CD11c (N418), CCR7 (4B12), CD169 (3D6.112), Ly6G (1A8), CD3 (17A2), NKp46 (29A1.4), Ki67 (16A8),

NK1.1 (PK136), Tim3 (RMT3–23), Granzyme B (QA17A02), FoxP3 (MF14), CD44 (1M7), IFN-γ (XMG1.2), CD107a (1D4B), CD62L (MEL-14), CD25 (PC61) and TNFα (MP6-XT22) were obtained from Biolegend. Antibodies to CD45 (30-F11), CD8α (53–6.7) and CD4 (GK1.5) were purchased from BD Biosciences. All antibodies were diluted 1:100. Gp70 tetramer (T-Select H-2L^d MuLV gp70 Tetramer-SPSYVYHQF-PE) was purchased from MBL. Tetramer staining was performed in buffer containing 50 nM dasatinib with 1:50 antibody dilution. Viability was assessed using Zombie Aqua and UV (Biolegend, 1:1000) for tumour and dLN samples or using DAPI for tetramer staining of blood samples. Intracellular staining for FoxP3, Ki67, IFN-γ, TNFα and Granzyme B was performed using the FoxP3 Transcription Factor Buffer Set (eBioscience).

B16F10 tumours and dLNs were harvested 1, 3, 6 or 9 days after i.t. treatment of day 8 tumours. Both were mechanically digested through 70 um nylon cell strainers to prepare single-cell suspensions. Blood was collected by submandibular bleeding into K2-EDTA tubes (Greiner-Bio) and red blood cells were lysed in ACK Lysis Buffer (Gibco). All samples were then resuspended in ice-cold PBS containing 1% (w/v) BSA and 2 mM EDTA (FACS buffer) with precision count beads (Biolegend, normalized to the weight of tissue per sample) before staining. For intracellular cytokine/granule staining of tumour and dLN infiltrating cells, digested tissue samples were resuspended in RPMI supplemented with 10% FBS, 1% penicillin-streptomycin, 1X non-essential amino acids (Invitrogen), 1X sodium pyruvate (Invitrogen), 1X 2-mercaptoethanol (Invitrogen) and 5 ug/mL brefeldin A (Sigma-Aldrich) for 4 hours at 37°C prior to staining. Cells were analyzed using BD FACS LSR Fortessa, or BD FACS Symphony A3 flow cytometers. Data were analyzed in FlowJo.

Statistics and reproducibility

Statistics were performed using Prism (GraphPad). Statistical methods were not used to determine sample size, but sample numbers were chosen based on estimates from pilot studies and published results, such that appropriate statistical tests would yield statistically significant results. For survival studies, log-rank (Mantel-Cox) tests were used. For FACS studies involving multiple time points, two-way ANOVAs followed by Tukey's multiple comparison tests were used while one-way ANOVAs or Student's t-tests were used for other experiments. The sample sizes for in vitro analysis were three and for in vivo analysis are as annotated in figure legends. The details of statistical analysis for figures and Supplementary Data figures are included in the Source Data files, which will be made available.

Supplementary Material

Refer to Web version on PubMed Central for supplementary material.

Acknowledgements

Y. Agarwal is partially supported by a graduate fellowship from the Ludwig Center at MIT's Koch Institute. D.J. Irvine is an investigator of the Howard Hughes Medical Institute. This work was supported by the Marble Center for Nanomedicine, the Ragon Institute of MGH, MIT, and Harvard, and by the Koch Institute Support (core) Grant P30-CA14051 from the National Cancer Institute. L.E. Milling and E.A. Lutz are supported by the NIGMS Biotechnology Training Grant T32GM833430, while L. Santollani, A. Sheen, E.A. Lutz, and A. Tabet are supported by the NSF Graduate Research Fellowship Program. L.E. Milling is also supported by Siebel Scholarship, L. Santollani is supported by the UCEM scholarship from the Alfred P. Sloan Foundation and A.

Tabet is supported by the Paul & Daisy Soros Fellowship. We thank the Koch Institute Swanson Biotechnology Center for technical support specifically the preclinical modeling, imaging & testing core facility, microscopy facility, histology facility, nanotechnology materials and the flow cytometry facility. We also thank H. Schreiber, R. Hynes and J. Scholm for critical reagents and all past and present members of Wittrup and Irvine laboratories for productive discussions and feedback regarding experiments and the manuscript. Some figures were created with BioRender.com.

Data availability

The main data supporting the results in this study are available within the paper and its Supplementary Information. Source data for the figures are provided with this paper. Any data supporting the findings of this study are also available from the corresponding authors on reasonable request.

References

1. Wolchok JD et al. Overall Survival with Combined Nivolumab and Ipilimumab in Advanced Melanoma. New England Journal of Medicine 377, 1345–1356 (2017). [PubMed: 28889792]
2. Ansell SM et al. PD-1 Blockade with Nivolumab in Relapsed or Refractory Hodgkin's Lymphoma. New England Journal of Medicine 372, 311–319 (2015). [PubMed: 25482239]
3. Brahmer J et al. Nivolumab versus Docetaxel in Advanced Squamous-Cell Non–Small-Cell Lung Cancer. New England Journal of Medicine 373, 123–135 (2015). [PubMed: 26028407]
4. Bellmunt J et al. Pembrolizumab as Second-Line Therapy for Advanced Urothelial Carcinoma. New England Journal of Medicine 376, 1015–1026 (2017). [PubMed: 28212060]
5. Yi M et al. Biomarkers for predicting efficacy of PD-1/PD-L1 inhibitors. Molecular Cancer vol. 17 1–14 (2018). [PubMed: 29304823]
6. Anderson KG, Stromnes IM & Greenberg PD Obstacles Posed by the Tumour Microenvironment to T cell Activity: A Case for Synergistic Therapies. Cancer Cell vol. 31 311–325 (2017). [PubMed: 28292435]
7. Smyth MJ, Ngiow SF, Ribas A & Teng MWL Combination cancer immunotherapies tailored to the tumour microenvironment. Nature Reviews Clinical Oncology vol. 13 143–158 (2016).
8. Moynihan KD et al. Eradication of large established tumours in mice by combination immunotherapy that engages innate and adaptive immune responses. Nature Medicine 22, 1402–1410 (2016).
9. Milling L, Zhang Y & Irvine DJ Delivering safer immunotherapies for cancer. Advanced Drug Delivery Reviews 114, 79–101 (2017). [PubMed: 28545888]
10. Lasek W, Zagożdżon R & Jakobisiak M Interleukin 12: Still a promising candidate for tumour immunotherapy? Cancer Immunology, Immunotherapy 63, 419–435 (2014). [PubMed: 24514955]
11. Kirchner GI et al. Pharmacokinetics of recombinant human interleukin-2 in advanced renal cell carcinoma patients following subcutaneous application. British Journal of Clinical Pharmacology 46, 5–10 (1998). [PubMed: 9690943]
12. June CH, Warshauer JT & Bluestone JA Is autoimmunity the Achilles' heel of cancer immunotherapy? Nature Medicine 23, 540–547 (2017).
13. Leonard John P., Sherman Matthew L., Fisher Gerald L., Buchanan Lynn J., Larsen Glenn, Atkins Michael B., Sosman Jeffrey A., Dutcher Janice P., Vogelzang Nicholas J., J. L. R. Effects of Single-Dose Interleukin-12 Exposure on Interleukin-12–Associated Toxicity and Interferon-γ Production. Blood 2541–2548 (1997) doi:10.1182. [PubMed: 9326219]
14. Atkins MB et al. Phase I evaluation of intravenous recombinant human interleukin 12 in patients with advanced malignancies. Clinical Cancer Research 3, (1997).
15. Melero I, Castanon E, Alvarez M, Champiat S & Marabelle A Intratumoural administration and tumour tissue targeting of cancer immunotherapies. Nature Reviews Clinical Oncology doi:10.1038/s41571-021-00507-y.
16. Aznar MA et al. Intratumoural Delivery of Immunotherapy—Act Locally, Think Globally. The Journal of Immunology 198, 31–39 (2017). [PubMed: 27994166]

17. Marabelle A, Kohrt H, Caux C & Levy R Intratumoural immunization: A new paradigm for cancer therapy. Clinical Cancer Research vol. 20 1747–1756 (2014). [PubMed: 24691639]
18. Brody JD et al. In situ vaccination with a TLR9 agonist induces systemic lymphoma regression: A phase I/II study. Journal of Clinical Oncology 28, 4324–4332 (2010). [PubMed: 20697067]
19. Posch C et al. Low-dose inhalation of interleukin-2 bio-chemotherapy for the treatment of pulmonary metastases in melanoma patients. British Journal of Cancer 110, 1427–1432 (2014). [PubMed: 24518593]
20. van Herpen CML et al. Intratumoural rhIL-12 administration in head and neck squamous cell carcinoma patients induces B cell activation. International Journal of Cancer 123, 2354–2361 (2008). [PubMed: 18729197]
21. Pfreundschuh MG et al. Phase I study of intratumoural application of recombinant human tumour necrosis factor. European Journal of Cancer and Clinical Oncology 25, (1989).
22. Nguyen KG et al. Localized Interleukin-12 for Cancer Immunotherapy. Frontiers in Immunology vol. 11 575597 (2020). [PubMed: 33178203]
23. Younes A et al. Phase II clinical trial of interleukin-12 in patients with relapsed and refractory non-Hodgkin's lymphoma and Hodgkin's disease. Clinical Cancer Research 10, 5432–5438 (2004). [PubMed: 15328181]
24. Little RF et al. Activity of subcutaneous interleukin-12 in AIDS-related Kaposi sarcoma. Blood 107, 4650–4657 (2006). [PubMed: 16507779]
25. Car BD, Eng VM, Lipman JM & Anderson TD The toxicology of interleukin-12: A review. in Toxicologic Pathology vol. 27 58–63 (Society of Toxicologic Pathologists, 1999). [PubMed: 10367675]
26. Li Y et al. Multifunctional oncolytic nanoparticles deliver self-replicating IL-12 RNA to eliminate established tumours and prime systemic immunity. Nature Cancer 1, 882–893 (2020). [PubMed: 34447945]
27. Chiocca EA et al. Regulatable interleukin-12 gene therapy in patients with recurrent high-grade glioma: Results of a phase 1 trial. Science Translational Medicine 11, (2019).
28. Momin N et al. Anchoring of intratumourally administered cytokines to collagen safely potentiates systemic cancer immunotherapy. Science Translational Medicine 11, eaaw2614 (2019). [PubMed: 31243150]
29. Flarend RE et al. In vivo absorption of aluminium-containing vaccine adjuvants using 26Al. Vaccine 15, 1314–1318 (1997). [PubMed: 9302736]
30. Morefield GL et al. Effect of phosphorylation of ovalbumin on adsorption by aluminum-containing adjuvants and elution upon exposure to interstitial fluid. Vaccine 23, 1502–1506 (2005). [PubMed: 15670886]
31. Moyer TJ et al. Engineered immunogen binding to alum adjuvant enhances humoral immunity. Nature Medicine 26, 430–440 (2020).
32. Hogenesch H, O'hagan DT & Fox CB Optimizing the utilization of aluminum adjuvants in vaccines: you might just get what you want. npj Vaccines 3, 51 (2018). [PubMed: 30323958]
33. Tagliabracci VS et al. A Single Kinase Generates the Majority of the Secreted Phosphoproteome. Cell 161, 1619–1632 (2015). [PubMed: 26091039]
34. Tagliabracci VS et al. Secreted Kinase Phosphorylates Extracellular Proteins That Regulate Biomineralization. Science 336, 1150–1153 (2012). [PubMed: 22582013]
35. Leonard JP et al. Effects of Single-Dose Interleukin-12 Exposure on Interleukin-12-Associated Toxicity and Interferon-g Production. http://ashpublications.org/blood/article-pdf/90/7/2541/1415768/2541.pdf.
36. Marabelle A, Tselikas L, de Baere T & Houot R Intratumoural immunotherapy: Using the tumour as the remedy. Annals of Oncology 28, xii33–xii43 (2017). [PubMed: 29253115]
37. Scrimieri F et al. Murine leukemia virus envelope gp70 is a shared biomarker for the high-sensitivity quantification of murine tumour burden. OncoImmunology 2, e26889 (2013). [PubMed: 24482753]
38. Garris CS et al. Successful Anti-PD-1 Cancer Immunotherapy Requires T Cell-Dendritic Cell Crosstalk Involving the Cytokines IFN-γ and IL-12. Immunity 49, 1148–1161.e7 (2018). [PubMed: 30552023]

39. Fallarino F, Ashikari A, Boon T & Gajewski TF Antigen-specific regression of established tumours induced by active immunization with irradiated IL-12- but not B7–1-transfected tumour cells. International Immunology 9, 1259–1269 (1997). [PubMed: 9310829]
40. Kerkar SP et al. IL-12 triggers a programmatic change in dysfunctional myeloid-derived cells within mouse tumours. Journal of Clinical Investigation 121, 4746–4757 (2011). [PubMed: 22056381]
41. Eisenbarth SC, Colegio OR, O'Connor W, Sutterwala FS & Flavell RA Crucial role for the Nalp3 inflammasome in the immunostimulatory properties of aluminium adjuvants. Nature 453, 1122–1126 (2008). [PubMed: 18496530]
42. Spranger S, Dai D, Horton B & Gajewski TF Tumour-Residing Batf3 Dendritic Cells Are Required for Effector T Cell Trafficking and Adoptive T Cell Therapy. Cancer Cell 31, 711–723.e4 (2017). [PubMed: 28486109]
43. Roberts EW et al. Critical Role for CD103 + /CD141 + Dendritic Cells Bearing CCR7 for Tumour Antigen Trafficking and Priming of T Cell Immunity in Melanoma HHS Public Access. Cancer Cell 30, 324–336 (2016). [PubMed: 27424807]
44. Broz ML et al. Dissecting the Tumour Myeloid Compartment Reveals Rare Activating Antigen-Presenting Cells Critical for T Cell Immunity. Cancer Cell 26, 638–652 (2014). [PubMed: 25446897]
45. Riley RS, June CH, Langer R & Mitchell MJ Delivery technologies for cancer immunotherapy. Nature Reviews Drug Discovery vol. 18 175–196 (2019). [PubMed: 30622344]
46. DA Z, KW H, CJ R, J S & JW G Intratumoural immunotherapy of established solid tumours with chitosan/IL-12. Journal of immunotherapy (Hagerstown, Md. : 1997) 33, 697–705 (2010). [PubMed: 20664357]
47. Wang C et al. In situ formed reactive oxygen species-responsive scaffold with gemcitabine and checkpoint inhibitor for combination therapy. Sci. Transl. Med 10, 3682 (2018).
48. Park CG et al. Extended release of perioperative immunotherapy prevents tumour recurrence and eliminates metastases. Science Translational Medicine 10, 1916 (2018).
49. Hori Y, Stern PJ, Hynes RO & Irvine DJ Engulfing tumours with synthetic extracellular matrices for cancer immunotherapy. Biomaterials 30, 6757–6767 (2009). [PubMed: 19766305]
50. Rahimian S et al. Polymeric microparticles for sustained and local delivery of antiCD40 and antiCTLA-4 in immunotherapy of cancer. Biomaterials 61, 33–40 (2015). [PubMed: 25993015]
51. Fransen MF, Sluijter M, Morreau H, Arens R & Melief CJM Local Activation of CD8 T Cells and Systemic Tumour Eradication without Toxicity via Slow Release and Local Delivery of Agonistic CD40 Antibody. Clinical Cancer Research 17, 2270–2280 (2011). [PubMed: 21389097]
52. Paulson JA et al. A facile approach to enhance antigen response for personalized cancer vaccination. Nature Materials 17, 528–534 (2018). [PubMed: 29507416]
53. Makvandi P et al. Stimuli-responsive transdermal microneedle patches. Materials Today (2021) doi:10.1016/J.MATTOD.2021.03.012.
54. Wang C, Ye Y, Hochu GM, Sadeghifar H & Gu Z Enhanced Cancer Immunotherapy by Microneedle Patch-Assisted Delivery of Anti-PD1 Antibody. (2016) doi:10.1021/acs.nanolett.5b05030.
55. Yang C, Blum NT, Lin J, Qu J & Huang P Biomaterial scaffold-based local drug delivery systems for cancer immunotherapy. Science Bulletin 65, 1489–1504 (2020).
56. Zhao Z et al. Delivery strategies of cancer immunotherapy: recent advances and future perspectives. Journal of Hematology & Oncology 2019 12:1 12, 1–14 (2019).
57. Xue K et al. Hydrogels as Emerging Materials for Translational Biomedicine. Advanced Therapeutics 2, 1800088 (2019).
58. C B et al. Improving therapeutic efficacy of IL-12 intratumoural gene electrotransfer through novel plasmid design and modified parameters. Gene therapy 25, 93–103 (2018). [PubMed: 29523878]
59. Champiat S et al. Intratumoural immunotherapy: From trial design to clinical practice. Clinical Cancer Research vol. 27 665–679 (2021). [PubMed: 32943460]
60. Kerkar SP et al. Collapse of the tumour stroma is triggered by IL-12 induction of Fas. Molecular Therapy 21, 1369–1377 (2013). [PubMed: 23568260]

61. Goldszmid RS et al. NK Cell-Derived Interferon-γ Orchestrates Cellular Dynamics and the Differentiation of Monocytes into Dendritic Cells at the Site of Infection. Immunity 36, 1047–1059 (2012). [PubMed: 22749354]

62. Nakahara T et al. Engagement of human monocyte-derived dendritic cells into interleukin (IL)-12 producers by IL-1β + interferon (IFN)-γ. Clinical and Experimental Immunology 139, 476–482 (2005). [PubMed: 15730393]

63. Hamid O et al. Alum with interleukin-12 augments immunity to a melanoma peptide vaccine: Correlation with time to relapse in patients with resected high-risk disease. Clinical Cancer Research 13, 215–222 (2007). [PubMed: 17200357]

64. Vilela L et al. Primate Model of Cutaneous Leishmaniasis Human IL-12 and Alum as Adjuvants in a Protective Immunity Using Recombinant. J Immunol References vol. 4481 http://www.jimmunol.org/content/163/8/http://www.jimmunol.org/content/163/8/4481.full#ref-list-1 (2021).

65. Klibanov AM Enzyme stabilization by immobilization. Analytical Biochemistry vol. 93 1–25 (1979). [PubMed: 35035]

66. Lauren CT, Belsito D. v., Morel KD & LaRussa P Case report of subcutaneous nodules and sterile abscesses due to delayed type hypersensitivity to aluminum-containing vaccines. Pediatrics 138, (2016).

67. Caspi RR Immunotherapy of autoimmunity and cancer: the penalty for success. Nature reviews. Immunology 8, 970 (2008).

68. Dudani JS, Warren AD & Bhatia SN Harnessing Protease Activity to Improve Cancer Care. Annual Review of Cancer Biology vol. 2 353–376 (2018).

69. Rothschilds AM & Dane Wittrup K What, Why, Where, and When: Bringing Timing to Immuno-Oncology. Trends in Immunology 40, 12–21 (2019). [PubMed: 30545676]

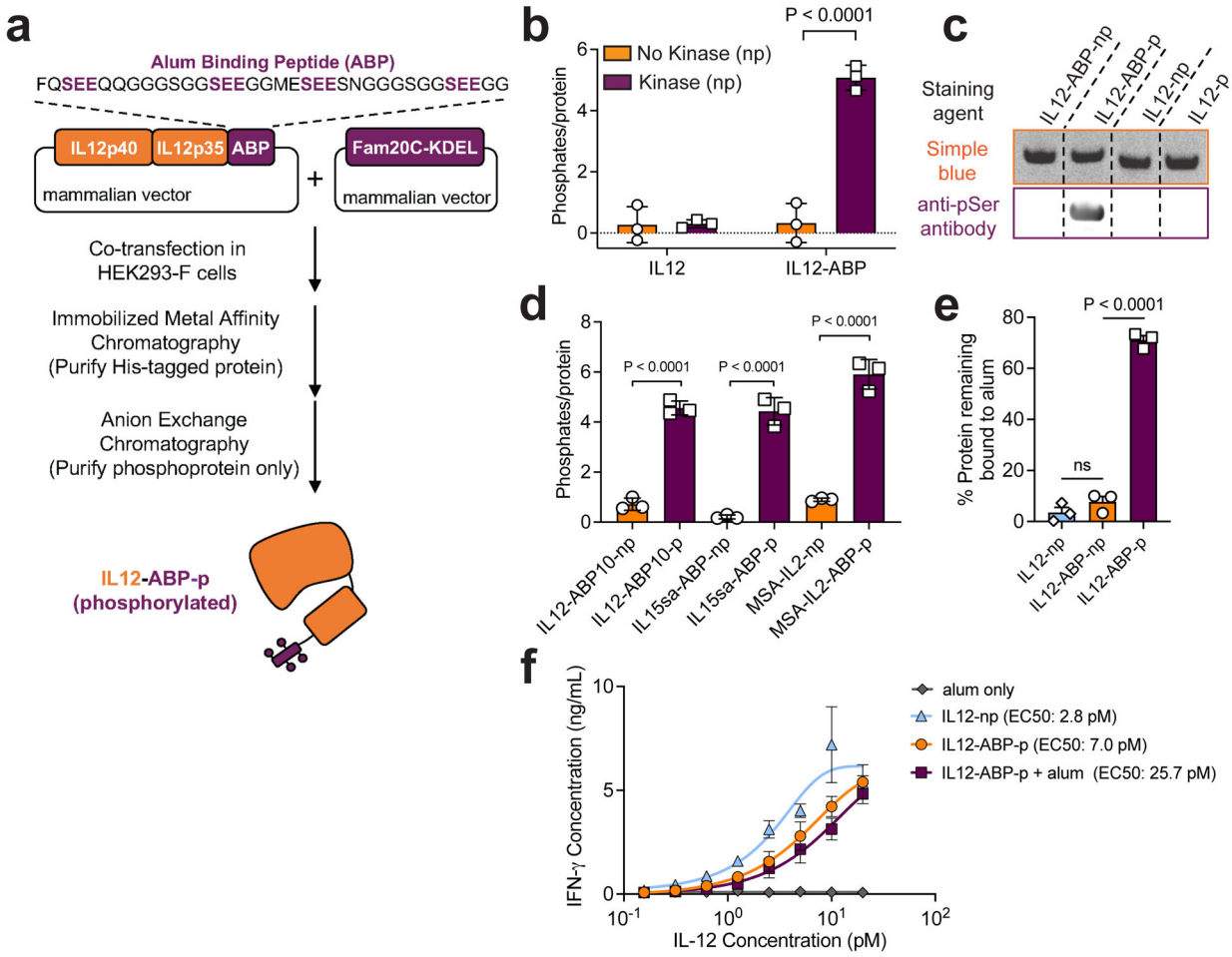

Fig. 1 |. Co-expression of cytokines and Fam20C enables in-cell site-specific serine phosphorylation of interleukins.

a, Manufacturing workflow for ABP-fusion proteins with IL-12 fused to ABP10 as an example. **b**, Phosphorylation as measured by malachite green assay for IL-12 and IL-12-ABP either expressed alone (np) or co-expressed with Fam20C-KDEL (p). **c**, Indicated proteins were run on an SDS-PAGE gel stained with Coomassie Blue (Simple Blue, orange) or transferred to a membrane and stained with an anti-pSer antibody followed by an IR800 secondary (purple). Shown are bands for ~65 kDa purified protein. The blot was analyzed by Fiji (ImageJ). The unedited blot image is available as Source Data. **d)** Phosphorylation was measured as in **b** for indicated proteins. **e)** Fluorophore-conjugated IL-12 fusion proteins (10 ug mL^{-1}) were mixed with Alhydrogel (100 ug mL^{-1}) for 30 mins in TBS, then incubated in 10% mouse serum in PBS for 1 h, followed by fluorescence spectroscopy to measure protein remaining bound to alum. **f)** IL-12 proteins at indicated concentrations (max alum concentration was 6 ng mL^{-1}) were incubated with murine splenocytes for 2 days. Shown are the IFN-γ concentrations measured in culture supernatants by ELISA. ABP refers specifically to ABP10. Data are representative of at least two independent experiments with n=3 technical replicates per group and presented as mean ± SD. P values were determined by ordinary one-way analysis of variance (ANOVA) followed by Tukey's

multiple comparison test (**c,e**) or two-way ANOVA with Šídák's multiple comparisons test (**b**) using GraphPad PRISM and exact P values are indicated (ns, not significant, $P > 0.05$).

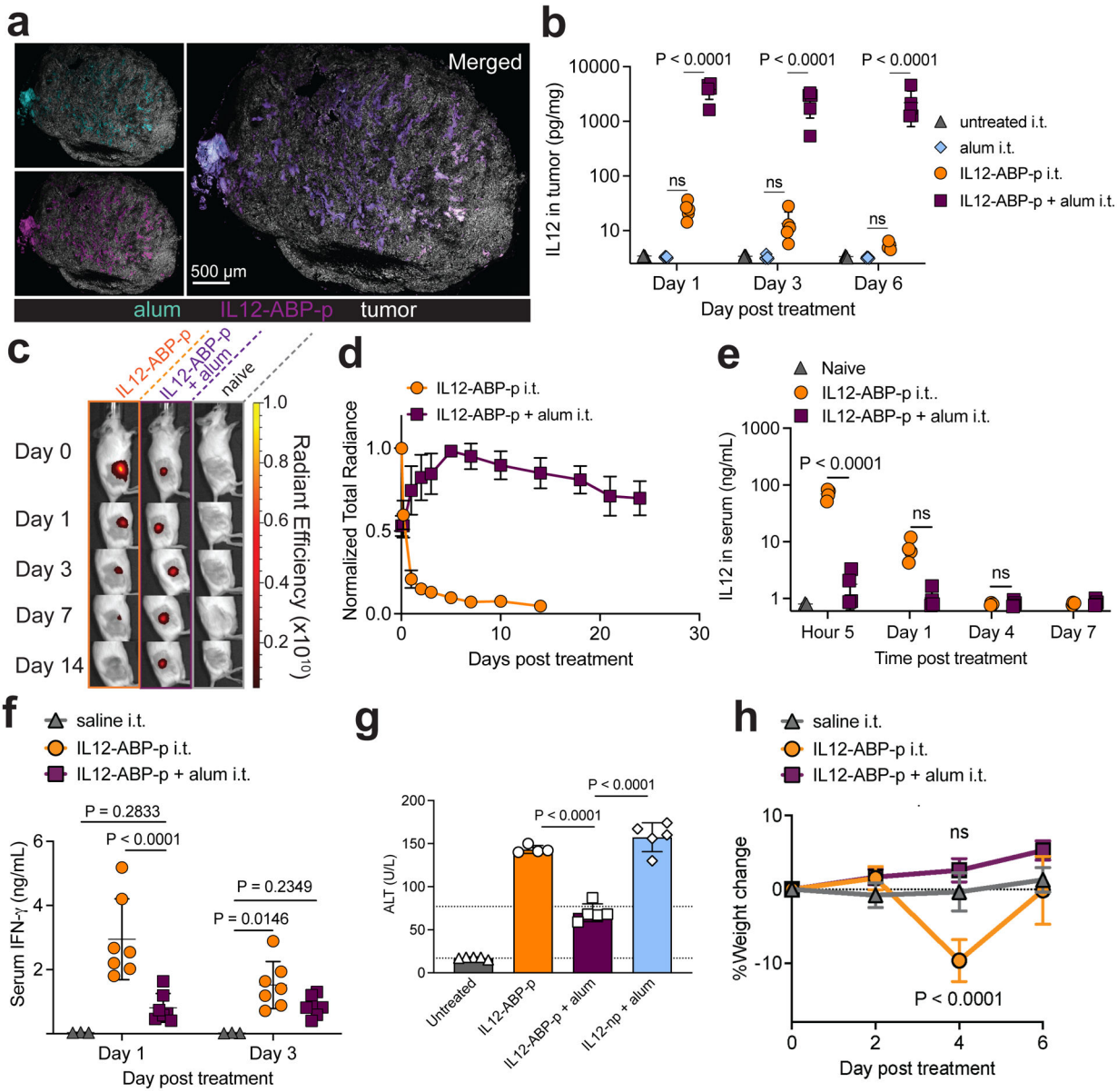

Fig. 2 |. Alum-tethered IL-12 is retained locally and elicits negligible systemic toxicity after intratumoural administration.

a-b, C57Bl/6 mice bearing s.c. B16F10 tumours were treated with 20 ug AF568-labeled IL-12-ABP-p + 100 μg AF488-pSer$_4$-labeled alum intratumourally (i.t.) (**a**) or 20 ug IL-12-ABP-p + 100 ug alum i.t. and 200 ug anti-PD1 intraperitoneally (i.p.) (**b**). Shown are representative tumour histological sections 30 minutes after injection with IL-2 in magenta, alum in cyan and B16F10 tumour cells in white; scale bars, 0.5 mm) (**a**) and IL-12 levels (n=5 animals/group) measured in tumour lysates at the indicated times (**b**). **c-e**, Albino B6 mice (n=4–5 animals/group) bearing s.c. B16F10-Trp2 KO (unpigmented) tumours were treated i.t. with 20 ug AF647-labelled IL-12-ABP-p alone (orange) or combined with 100 ug alum (purple). Shown are the representative IVIS images (**c**), quantification of intratumoural AF647 fluorescence (**d**) and serum IL-12 levels (**e**) over time. **f-h**, C3H-Hej mice (n=5–7

animals/group) with established Ag104A tumours were treated i.t. with 20 μg IL-12 alone, 20 μg IL-12-ABP-p alone, or IL-12-ABP-p mixed with 100 μg alum. Shown are serum IFN-γ levels (**f**), serum ALT concentration on day 3 post-treatment (**g**) and % change in body weight over time after treatment (**h**). All data are presented as mean ± SD with indicated n. ABP refers specifically to ABP10. P values were determined by ordinary one-way ANOVA (**g**) or two-way ANOVA (**b, f, h**) followed by Tukey's multiple comparison test, and two-way ANOVA followed by Holm-Šídák multiple comparison test (**e**) using GraphPad PRISM and exact P values are indicated. P values for **h** were computed versus the saline i.t. group. ns, not significant or $P > 0.05$.

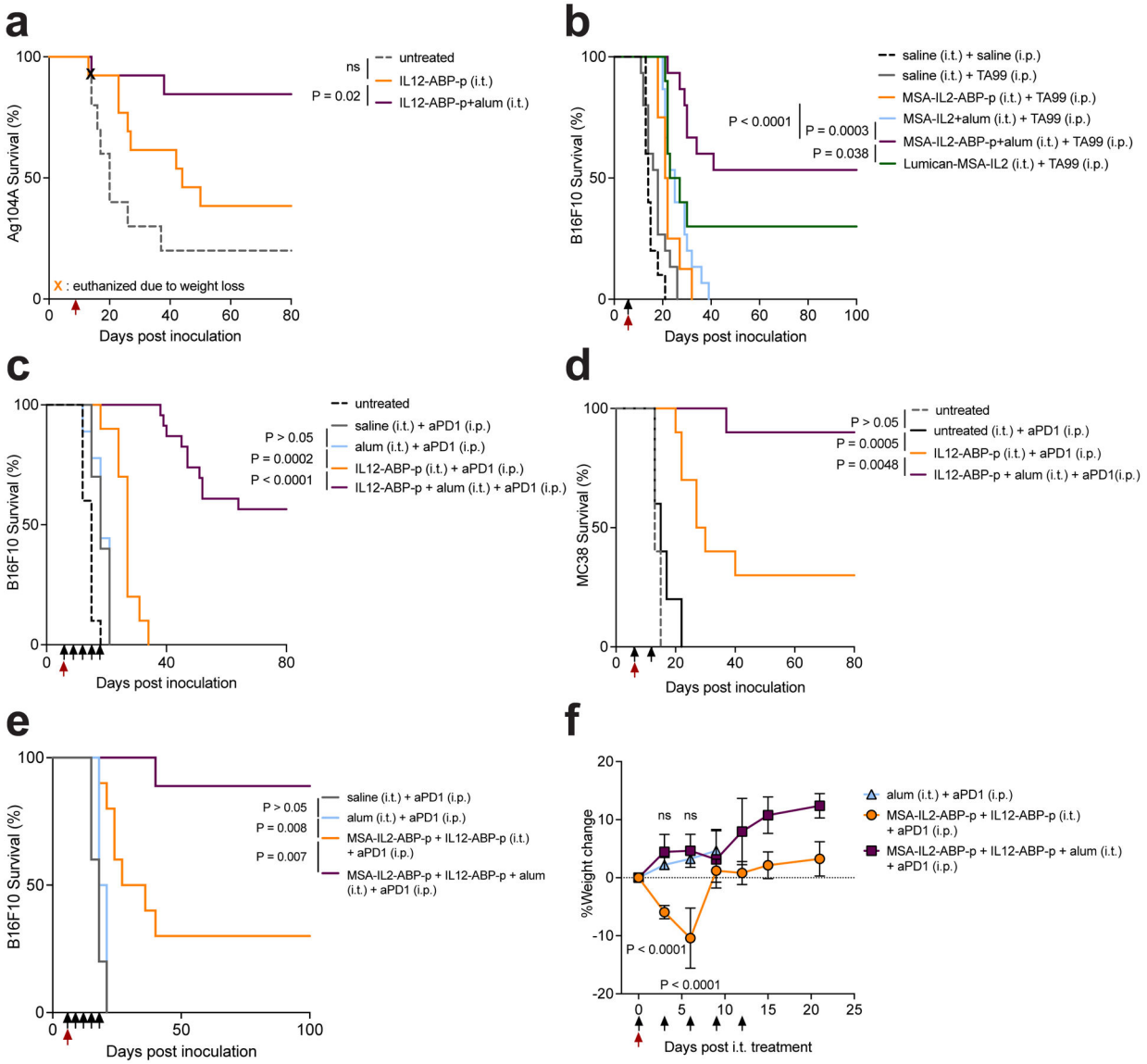

Fig. 3 |. A single dose of alum-anchored intratumoural IL-12 or IL-2 elicits long-term tumour regression in multiple syngeneic cancer models.

a-d, Overall survival over time for mice bearing flank Ag104A (**a**), B16F10 (**b-c**) or MC38 (**d**) tumours after a single i.t. dose administered on day 7 (**a, d**) or day 6 (**b-c**) after inoculation. Groups for **a** were untreated (n=10), IL-12-ABP-p (20 μg) i.t. (n=13), and IL-12-ABP-p (20 μg)/alum (100 μg) i.t. (n=13). Treatments for **b** were saline i.t. + saline i.p. (n=10), saline i.t. + TA99 i.p. (n=15), MSA-IL-2-ABP-p (36 μg) i.t. + TA99 i.p. (n=8), MSA-IL-2(34 μg)/alum (90 μg) i.t. + TA99 i.p. (n=15), MSA-IL-2-ABP-p (36 μg)/alum (90 μg) i.t. + TA99 i.p. (n=15), and Lumican-MSA-IL-2 (52 μg) i.t. + TA99 i.p. (n=10). TA99 was dosed at 200 μg per injection. Treatments for **c** were untreated (n=10), saline i.t. + anti-PD1 i.p. (n=10), alum (100 ug) i.t. + anti-PD1 i.p. (n=9), IL-12-ABP-p (20 ug) i.t. (n=15), and IL-12-ABP-p (20 ug)/alum (100 ug) i.t (n=28). Treatments for **d** were untreated (n=5), untreated i.t. + anti-PD1 i.p. (n=5), IL-12-ABP-p (20 ug) i.t. (n=10), and IL-12-ABP-p (20 ug)/alum (100 ug) i.t (n=20). Anti-PD1 was dosed at 200 μg per

injection. **e-f**, Mice with B16F10 tumours were treated on day 6 i.t. with saline (n=5), alum (100 ug, n=5), IL-12-ABP-p (20 ug) + MSA-IL-2-ABP-p (36 ug, n=10), or IL-12-ABP-p + MSA-IL-2-ABP-p + alum (n=10); all groups received anti-PD1 i.p. (black arrowheads). Shown is the overall survival (e) and percent change in body weight (mean ± SD, **f**) over time after treatment. Anti-PD1 was administered on days 6, 9, 12, 15 and 18 for **b, f, g** and days 7, 13 for **c**. Red and black arrowheads indicate timing of i.t. and i.p. treatments respectively. ABP refers specifically to ABP10. P values were determined by the log-rank (Mantel-Cox) test (**a,c-d**), Gehan-Breslow-Wilcoxon test (**b,e**) or two-way ANOVA followed by Tukey's multiple comparison test versus alum i.t. at indicated time points (**f**) using GraphPad PRISM. ns, not significant or $P > 0.05$.

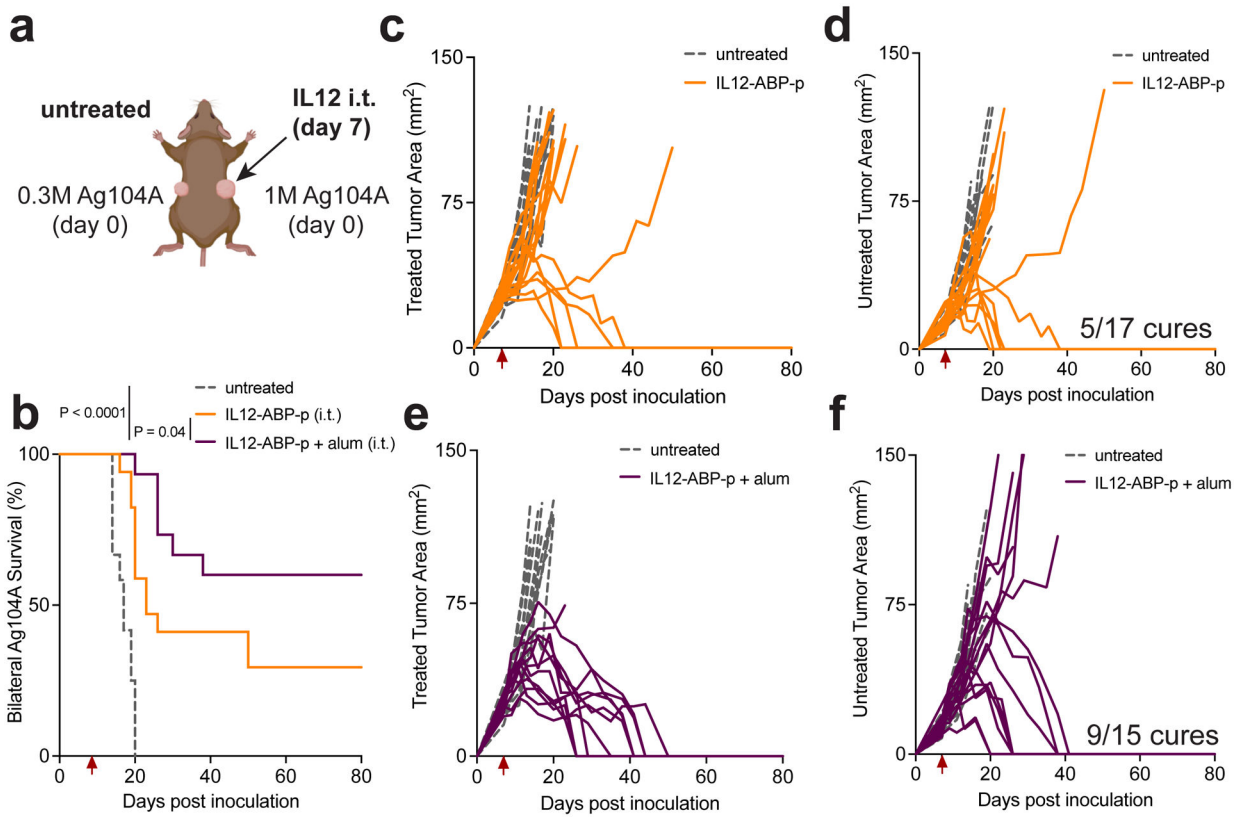

Fig. 4 |. A single local dose of anchored IL-12 controls distal, untreated tumours.

a-f, C3H-Hej mice (untreated n = 10 mice/group, IL-12-ABP-p i.t. n=17 mice/group and IL-12-ABP-p + alum i.t. n=15 mice/group) were inoculated subcutaneously (s.c.) with 10^6 and 0.3×10^6 Ag104A cells on the right and left flanks, respectively. At day 7, the right flank tumour was treated i.t. with 20 ug IL-12-ABP-p alone or mixed with 100 ug alum. Shown is the experimental setup (**a**), overall mouse survival (**b**), and individual tumour growth curves for treated (**c, e**) and untreated (**d, f**) tumours. Red arrows indicate timing of i.t. treatments. ABP refers specifically to ABP10. P values were determined by the log-rank (Mantel-Cox) test (**b**) using GraphPad PRISM.

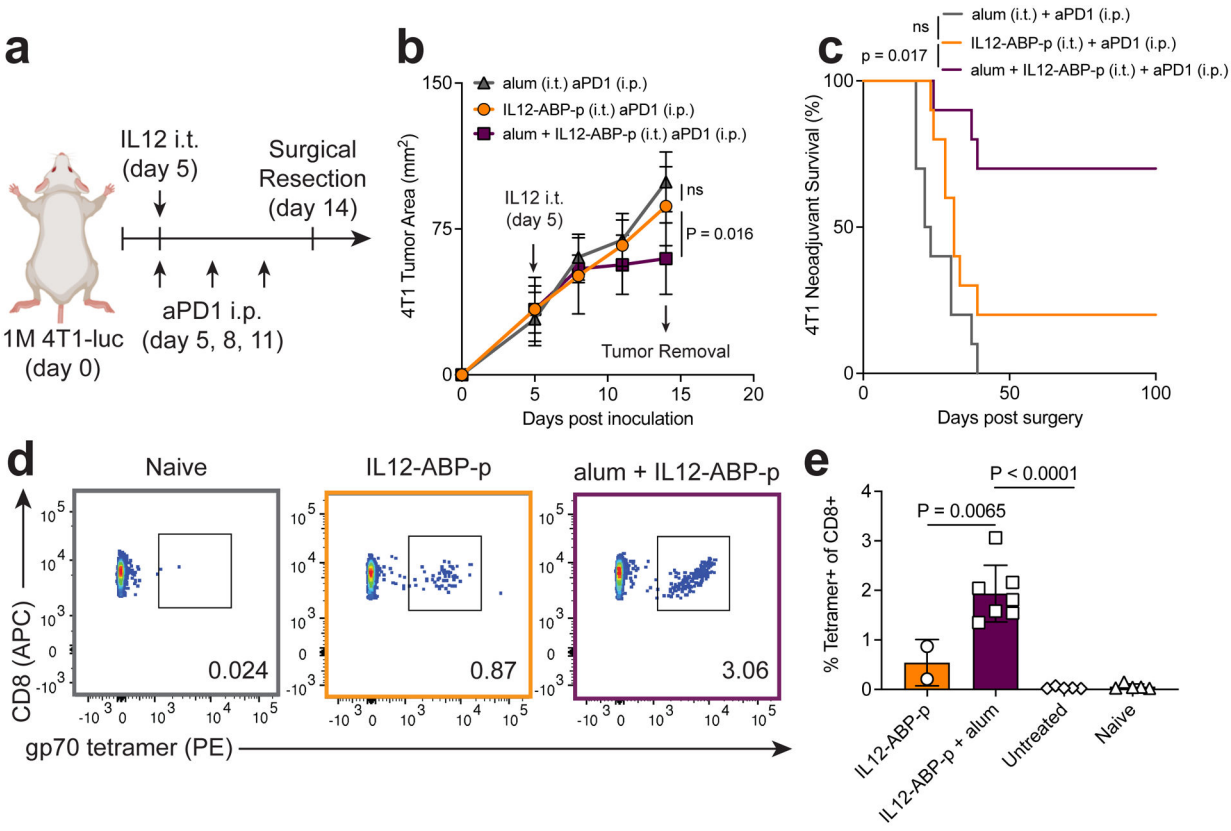

Fig. 5 |. Neoadjuvant alum/IL12 promotes systemic immunity in the orthotopic 4T1 breast cancer model.

a-e, BALB/c mice (n = 10 mice for all groups) were inoculated with 0.5×10^6 4T1-luc cells orthotopically in the mammary fat pad and 5 days later, tumours were treated i.t. with 20 ug IL-12-ABP-p, 100 ug alum or a combination of the two. Mice were also treated with 200 ug anti-PD1 i.p. on days 5, 8 and 11. On day 14, primary tumours were surgically removed. Shown is the experimental timeline (**a**), primary tumour growth (mean ± SD, **b**), and overall survival (**c**). On day 56, peripheral blood of surviving mice (IL-12-ABP-p, n = 2 and IL-12-ABP-p/alum, n = 7), naïve mice (n=5), and untreated animals bearing 14-day old orthotopic 4T1 tumours (n=5) was analyzed by flow cytometry. Shown are representative flow plots (**d**) and quantification of gp70 tetramer$^+$CD8$^+$ T cells (**e**) in the peripheral blood. ABP refers specifically to ABP10. P values were determined by the log-rank (Mantel-Cox) test (**c**) and one-way (**e**) or two-way (**b**) ANOVA followed by Tukey's multiple comparison test using GraphPad PRISM. ns, not significant or P > 0.05.

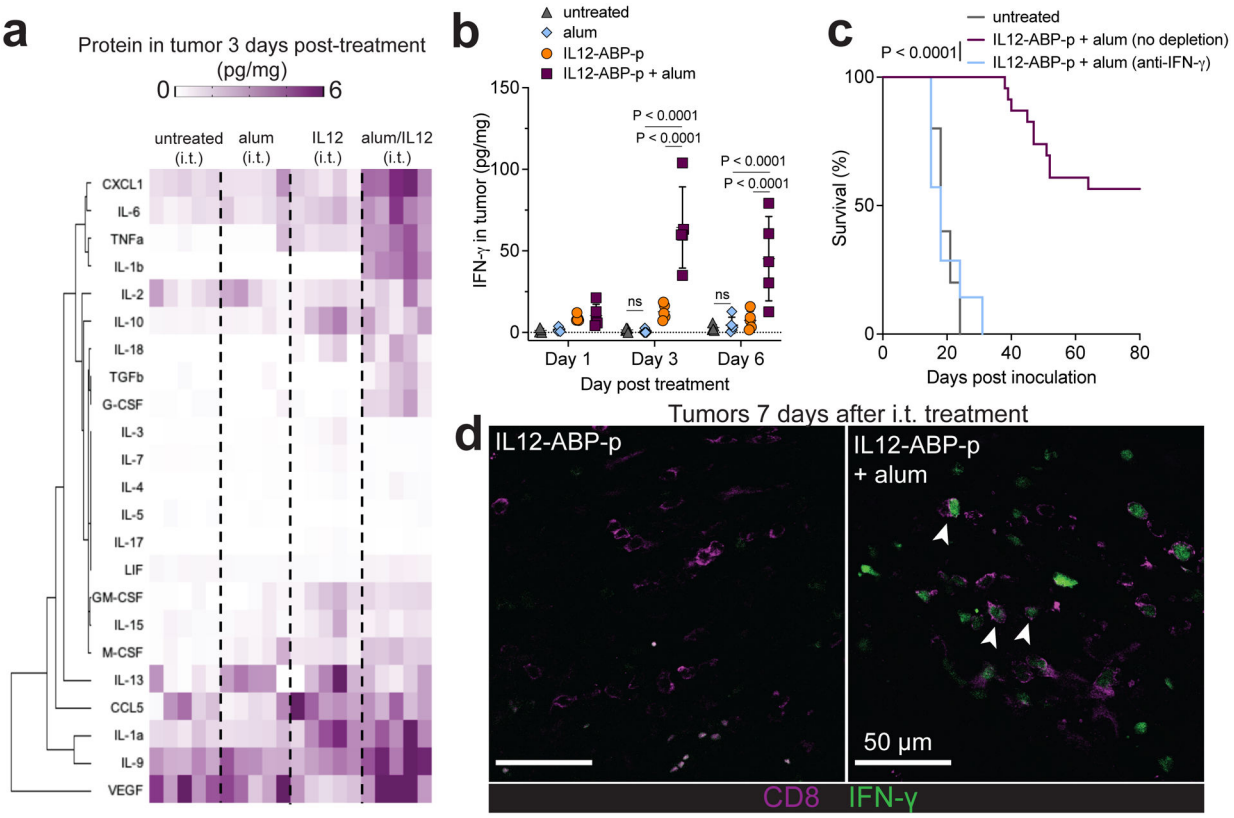

Fig. 6 |. IFN-γ production is critical for alum-anchored IL-12-mediated tumour rejection.

a-b, Mice were inoculated s.c. in the flank with 10^6 B16F10 tumour cells and treated on day 6 with no i.t. treatment (n=5 mice per group), alum (100 ug) i.t., IL-12-ABP-p (20 ug) i.t. or IL-12-ABP-p (20 ug) + alum (100 ug) i.t. combined with systemic anti-PD1 (200 ug per dose) on days 6 and 9. Tumours were isolated and cytokine/chemokine levels were quantified by Luminex 3 days post treatment (**a**) and IFN-γ amounts in tumours 1, 3 or 6 days after treatment were quantified by ELISA (mean ± SD, **b**). **c**, Overall survival for mice bearing B16F10 tumours and treated as in **a** in the presence or absence of anti-IFN-γ starting 1d before i.t. treatment and every 2d thereafter (untreated n=10 mice/group, treated n=23 mice/group, and treated + anti-IFN-γ n=7 mice/group). **d**, IFN-γ reporter mice bearing B16F10 tumours were treated as in **a** with AF405-labeled IL-12-ABP-p alone or combined with alum. Shown are representative histological tumour cross sections 7 days after treatment with IFN-γ in green and CD8 in magenta (n = 3 mice/group; scale bars, 50 um, white arrows point to IFN-γ^+CD8$^+$ T cells). ABP refers specifically to ABP10. P values were determined by the log-rank (Mantel-Cox) test (**c**) and two-way (**b**) ANOVA followed by Tukey's multiple comparison test using GraphPad PRISM.

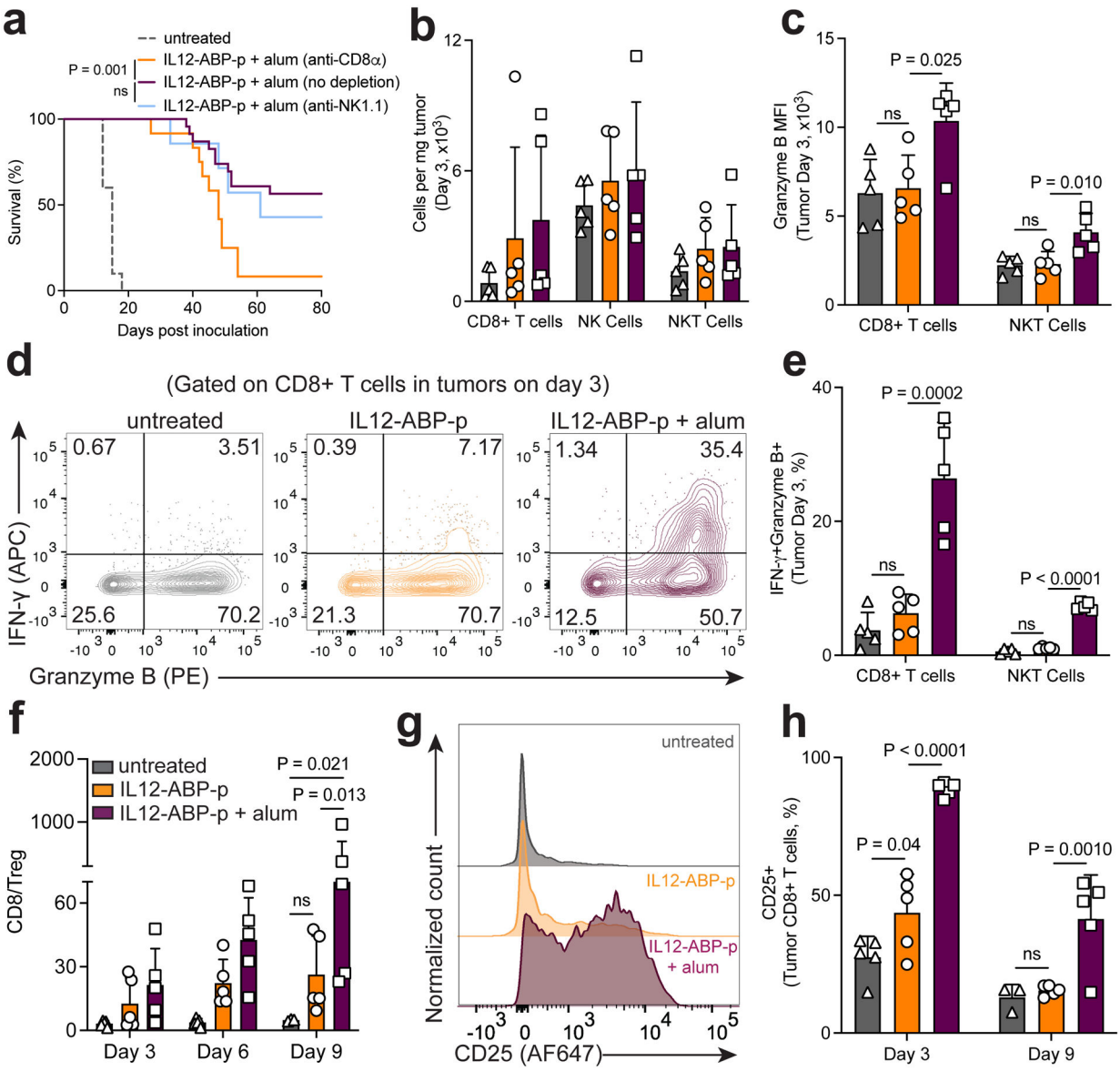

Fig. 7 |. Single-dose alum/IL12 therapy enhances intratumoural T and NKT cell activity.

a, Overall survival for mice bearing B16F10 tumours treated as in Fig. 3c that were also administered depleting antibodies starting 1 day before treatment and every 3d thereafter (untreated n=10 mice/group, treated n=23 mice/group, treated + anti-CD8α n = 12 mice/group, and treated + anti-NK1.1 n=7 mice per group). **b-h**, Mice bearing B16F10 tumours (n=5 mice per group) were treated as in Fig. 6a. Tumours were analyzed on days 3, 6 and 9 after treatment by flow cytometry. Shown are the quantification of tumour-infiltrating $CD8^+$ T, NK and NKT cells (mean ± SD, **b**), granzyme B geometric MFI (**c**), representative flow plots for intratumoural $CD8^+$ T cells (**d**), and enumeration (mean ± SD) of intratumoural IFN-γ^+granzyme B^+ $CD8^+$ T and NKT cells (**e**) on day 3. **f**, Ratio of $CD8^+$ T cell counts to $FoxP3^+CD25^+$ Treg counts over time (mean ± SD). **g-h**, Representative day 3 flow plots (**g**) and quantification (mean ± SD, **h**) of CD25 expression by intratumoural $CD8^+$ T cells. ABP refers specifically to ABP10. P values were determined by the log-rank (Mantel-Cox) test

(**a**) and one-way (**c,e**) or two-way (**f,h**) ANOVA followed by Tukey's multiple comparison test using GraphPad PRISM. ns, not significant or $P > 0.05$.

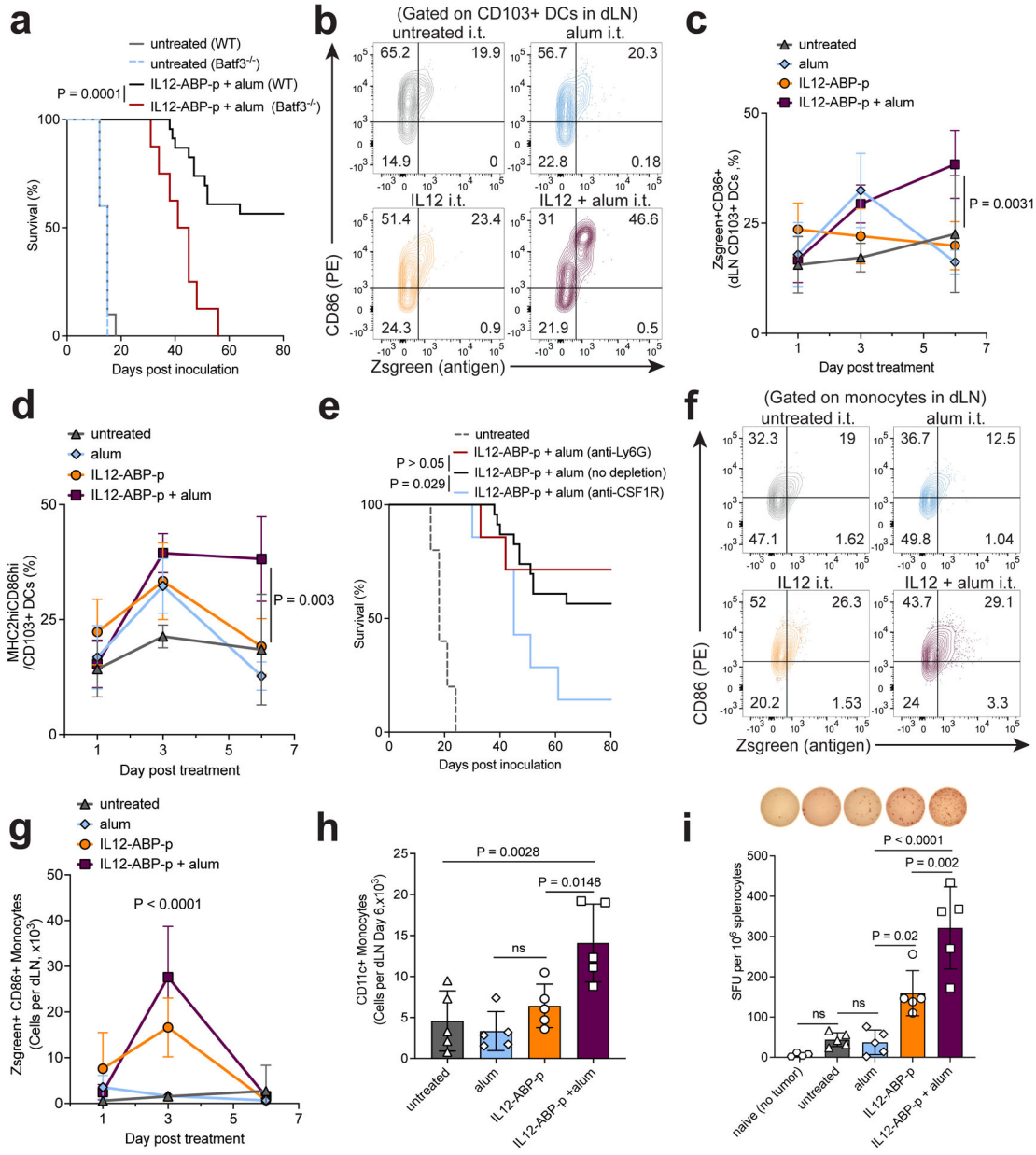

Fig. 8 |. Intratumourally persistent IL-12 promotes tumour antigen accumulation in activated draining lymph node APCs.

a, Overall survival for B16F10-bearing wild-type (WT) or *Batf3*$^{-/-}$ mice (Untreated WT n =10 mice/group, untreated *Batf3*$^{-/-}$ n=5 mice/group, IL-12-ABP-p + alum WT n = 23 mice/group, and IL-12-ABP-p + alum *Batf3*$^{-/-}$ n=8 mice/group) treated as in Fig. 3c with indicated proteins i.t. and anti-PD1 i.p. every 3 days after. **b-d**, Mice bearing B16F10-Zsgreen tumours (n=5–7 mice/group) were treated i.t. as indicated and i.p. with anti-PD1 every 3 days after treatment. CD103^{+} DCs in draining lymph nodes (dLN) were analyzed by flow cytometry 1, 3 or 6 days after treatment. Shown are representative day 6 flow plots (**b**) and quantification (mean ± SD, **c**) for CD103^{+} DCs positive for both zsgreen and CD86 and proportion of MHC-II^{hi}CD86^{hi} CD103^{+} DCs (mean ± SD, **d**). **e**, Overall survival for mice bearing B16F10 tumours treated as in Fig. 3c that were also administered

depleting antibodies starting 1 day before treatment and every 3d thereafter (untreated n=10 mice/group, treated n=23 mice/group, treated + anti-Ly6G n = 7 mice/group, treated + anti-CSF1R n = 7 mice/group). **f-h**, dLN monocytes were analyzed as in **b-d**. Shown are representative day 3 flow plots (**f**), enumeration of $Zsgreen^{+}CD86^{hi}$ monocytes over time (mean ± SD, **g**), and enumeration of CD11c+ monocytes at day 6 (mean ± SD, **h**). **i**, B16F10-bearing mice (n=5) were treated i.t. as in Fig. 3c with indicated combinations and i.p. with anti-PD1 every 3 days. At day 10 post treatment, splenocytes were isolated and stimulated with irradiated B16F10 cells in an IFN- γ ELISPOT assay. Shown is the number of spot-forming units (SFU) per 10^6 splenocytes plated per group (mean ± SD) and representative images of ELISPOT wells. ABP refers specifically to ABP10. P values were determined by the log-rank (Mantel-Cox) test (**a,e**) and one-way (**h,i**) or two-way (**c,d,g**) ANOVA followed by Tukey's multiple comparison test using GraphPad PRISM. ns, not significant or $P > 0.05$.